Alaska Department of Transportation & Public Facilities
Alaska University Transportation Center

Laboratory Performance of Wicking Fabric H2Ri in Silty Gravel, Sand and Organic Silt

Billy Connor, P.E.
Xiong Zhang, P.E., Ph.D.
University of Alaska Fairbanks

May 2016

Alaska University Transportation Center
Duckering Building Room 245
P.O. Box 755900
Fairbanks, AK 99775-5900

Alaska Department of Transportation
Research, Development, and Technology Transfer
PO Box 112500
3132 Channel Drive
Juneau, Alaska 99811-2500

INE/AUTC 16.04

DOT&PF Report No. 4000130

Notice

This document is disseminated under the sponsorship of the U.S. Department of Transportation in the interest of information exchange. The U.S. Government assumes no liability for the use of the information contained in this document. The U.S. Government does not endorse products or manufacturers. Trademarks or manufacturers' names appear in this report only because they are considered essential to the objective of the document.

Quality Assurance Statement

The Federal Highway Administration (FHWA) provides high-quality information to serve Government, industry, and the public in a manner that promotes public understanding. Standards and policies are used to ensure and maximize the quality, objectivity, utility, and integrity of its information. FHWA periodically reviews quality issues and adjusts its programs and processes to ensure continuous quality improvement.

Author's Disclaimer

Opinions and conclusions expressed or implied in the report are those of the authors. They are not necessarily those of the Alaska DOT&PF or funding agencies.

REPORT DOCUMENTATION PAGE

Form approved OMB No.

1. AGENCY USE ONLY (LEAVE BLANK)	2. REPORT DATE	3. REPORT TYPE AND DATES COVERED
Report No. 4000130	May 2016	Final Report

4. TITLE AND SUBTITLE
Laboratory Performance of Wicking Fabric H2Ri in Sandy Gravel, Sand and Organic Silt

5. FUNDING NUMBERS
Alaska DOT&PF: Z630410000

AUTC: G8085 Fund 338035

6. AUTHOR(S)
Billy Connor, PE
Xiong Zhang, Ph.D., PE

7. PERFORMING ORGANIZATION NAME(S) AND ADDRESS(ES)
Alaska University Transportation Center
University of Alaska Fairbanks
Duckering Building Room 245
P.O. Box 755900
Fairbanks, AK 99775-5900

8. PERFORMING ORGANIZATION REPORT NUMBER
INE/AUTC

9. SPONSORING/MONITORING AGENCY NAME(S) AND ADDRESS(ES)
Department of Transportation & Public Facilities
Research, Development, and Technology Transfer
PO Box 112500
3132 Channel Drive
Juneau, Alaska 99811-2500

10. SPONSORING/MONITORING AGENCY REPORT NUMBER
Report # 4000130

11. SUPPLENMENTARY NOTES

12a. DISTRIBUTION / AVAILABILITY STATEMENT
No restrictions

12b. DISTRIBUTION CODE

13. ABSTRACT (Maximum 200 words)

The use of wicking fabric, H2Ri, is growing in its use to remove water from roadway and airport embankments. Past research has shown H2Ri to be effective in sands and fine grained materials in roadways up to 32 feet in width. However, there is a desire to use H2Ri for airports which require a minimum width of 75 ft. This project tested H2Ri in a 73-foot flume in a crushed surface course with 14 % fines. In addition, the fabric was tested in a 22-foot flume with a sand and with an organic clay. The intent was to bracket the material for which the H2Ri will work. The study showed that the fabric will easily move water 73 feet in a silty gravel. The study showed that the fabric was also able to readily remove water in sand. However, the fabric blinded when used in organic silt and proved ineffective.

The study also showed that using simple overlap of the H2Ri as a splice, while effective, was not as efficient at moving water as the fabric itself. Consequently, moisture tended to build up around the splice.

14- KEYWORDS: Geosynthetics (Rbmdxce), Unsaturated soils (Rbespmy), silts(Rbesgt), Sand (Rbesgs); Wicking Fabric

15. NUMBER OF PAGES
70

16. PRICE CODE
N/A

17. SECURITY CLASSIFICATION OF REPORT	18. SECURITY CLASSIFICATION OF THIS PAGE	19. SECURITY CLASSIFICATION OF ABSTRACT	20. LIMITATION OF ABSTRACT
Unclassified	Unclassified	Unclassified	N/A

NSN 7540-01-280-5500

STANDARD FORM 298 (Rev. 2-98)
Prescribed by ANSI Std. 239-18 298-1

SI* (MODERN METRIC) CONVERSION FACTORS

APPROXIMATE CONVERSIONS TO SI UNITS

Symbol	When You Know	Multiply By	To Find	Symbol
		LENGTH		
in	inches	25.4	millimeters	mm
ft	feet	0.305	meters	m
yd	yards	0.914	meters	m
mi	miles	1.61	kilometers	km
		AREA		
in^2	square inches	645.2	square millimeters	mm^2
ft^2	square feet	0.093	square meters	m^2
yd^2	square yard	0.836	square meters	m^2
ac	acres	0.405	hectares	ha
mi^2	square miles	2.59	square kilometers	km^2
		VOLUME		
fl oz	fluid ounces	29.57	milliliters	mL
gal	gallons	3.785	liters	L
ft^3	cubic feet	0.028	cubic meters	m^3
yd^3	cubic yards	0.765	cubic meters NOTE: volumes greater than 1000 L shall be	m^3
		MASS		
oz	ounces	28.35	grams	g
lb	pounds	0.454	kilograms	kg
T	short tons (2000 lb)	0.907	megagrams (or "metric ton")	Mg (or "t")
		TEMPERATURE (exact degrees)		
°F	Fahrenheit	5 (F-32)/9 or (F-32)/1.8	Celsius	°C
		ILLUMINATION		
fc	foot-candles	10.76	lux	lx
fl	foot-Lamberts	3.426	$candela/m^2$	cd/m^2
		FORCE and PRESSURE or STRESS		
lbf	poundforce	4.45	newtons	N
lbf/in^2	poundforce per square inch	6.89	kilopascals	kPa

APPROXIMATE CONVERSIONS FROM SI UNITS

Symbol	When You Know	Multiply By	To Find	Symbol
		LENGTH		
mm	millimeters	0.039	inches	in
m	meters	3.28	feet	ft
m	meters	1.09	yards	yd
km	kilometers	0.621	miles	mi
		AREA		
mm^2	square millimeters	0.0016	square inches	in^2
m^2	square meters	10.764	square feet	ft^2
m^2	square meters	1.195	square yards	yd^2
ha	hectares	2.47	acres	ac
km^2	square kilometers	0.386	square miles	mi^2
		VOLUME		
mL	milliliters	0.034	fluid ounces	fl oz
L	liters	0.264	gallons	gal
m^3	cubic meters	35.314	cubic feet	ft^3
m^3	cubic meters	1.307	cubic yards	yd^3
		MASS		
g	grams	0.035	ounces	oz
kg	kilograms	2.202	pounds	lb
Mg (or "t")	megagrams (or "metric ton")	1.103	short tons (2000 lb)	T
		TEMPERATURE (exact degrees)		
°C	Celsius	1.8C+32	Fahrenheit	°F
		ILLUMINATION		
lx	lux	0.0929	foot-candles	fc
cd/m^2	$candela/m^2$	0.2919	foot-Lamberts	fl
		FORCE and PRESSURE or STRESS		
N	newtons	0.225	poundforce	lbf
kPa	kilopascals	0.145	poundforce per square inc h	lbf/in^2

*SI is the symbol for the International System of Units. Appropriate rounding should be made to comply with Section 4 of ASTM E380.
(Revised March 2003)

Table of Contents

LIST OF FIGURES

LIST OF TABLES

CHAPTER I INTRODUCTION

A wicking fabric referred to as H2Ri is gaining popularity for removing moisture from roadway embankments. Alaska's first experience with using this material was at Beaver Slide, Milepost (MP) 110.5 on the Dalton Highway. Beaver Slide has been problematic since its construction in 1975. The site is situated on a sidehill cut with a roadway grade that exceeds 6%. The soil at Beaver Slide is dense grade sand with gravel; about 6% passes the #200 sieve. This soil combination allowed water to move across and along the road, causing wet soft spots in the roadway. Freeze-thaw activity exacerbated the problem, but installation of H2Ri eliminated it. For 5 years, the roadway has been free of soft spots.

The Alaska Department of Transportation and Public Facilities (DOT&PF) used H2Ri on another Dalton Highway project at MP 197 - 209. To date that roadway has not developed problems. However, Alaska DOT&PF has asked two questions:

1. Are there soil types in which H2Ri is not effective?
2. Will H2Ri continue to work when length requirements exceed the width of the wicking fabric?

This study answers the questions. Two materials were used to represent the extreme conditions in which H2Ri might be used. The first material was a free-draining clean, uniform sand. This material provided an understanding of how well H2Ri works in permeable soil.

The second material was an organic silt obtained from the CRREL Permafrost Tunnel near Fox, Alaska, just north of Fairbanks. Organic silt is essentially impervious, providing an understanding of the performance of H2Ri in impermeable soil.

CHAPTER 2 LITERATURE REVIEW

2.1 Adverse Effects of Subsurface Water in Pavement Design

Excessive water in a pavement structure is recognized as one of the major adverse factors that influence pavement's overall performance. Excess water can cause a variety of engineering problems. Soil expansion and collapse, soil strength reduction and soil stiffness, increase in excess pore water pressure and development of seepage force, asphalt pavement stripping, and crack generation all can be caused by excess water (Han and Zhang, 2014). Figure 2.1 shows the mechanism of water-induced asphalt concrete (AC) pavement distress (Taylor and Khosla, 1983). Both dynamic traffic load and thermal shrinkage induce cracks within the asphalt pavement layer. Cracks partially or completely fill with water through infiltration, which, over time, results in saturation of base and subgrade materials. Higher pore water pressure is induced by large dynamic loading of heavy-duty vehicles. In consequence, free water within the base and subgrade, together with fines, are squeezed out of the pavement structure. This phenomenon is called pumping. Free water wedges are produced beneath the asphalt pavement. Wet softened areas due to loss of fines in the base and subgrade layers cause potholes or depressions of the pavement structure. Similar pumping phenomena occur in Portland cement concrete (PCC) pavements (Mallela et al., 2000), as shown in Figure 2.2. Upward curling of pavement slabs (resulting from uneven temperatures above and beneath a cement pavement slab) tends to create small pores. Free water can easily penetrate and saturate base and subgrade layers via joints through precipitation and infiltration. The oncoming wheel load causes the backward slab edge to deflect downward, generating large pore water pressure. When the wheel passes the joint, the forward slab deflects downward, and the slab that the wheel load has passed rebounds upward. The cyclic downward deflecting–upward rebounding process pumps water out of the pavement structure together with fines. The materials beneath the joints of slabs erode with time, and faults or cracks near joints further accelerate the deterioration process.

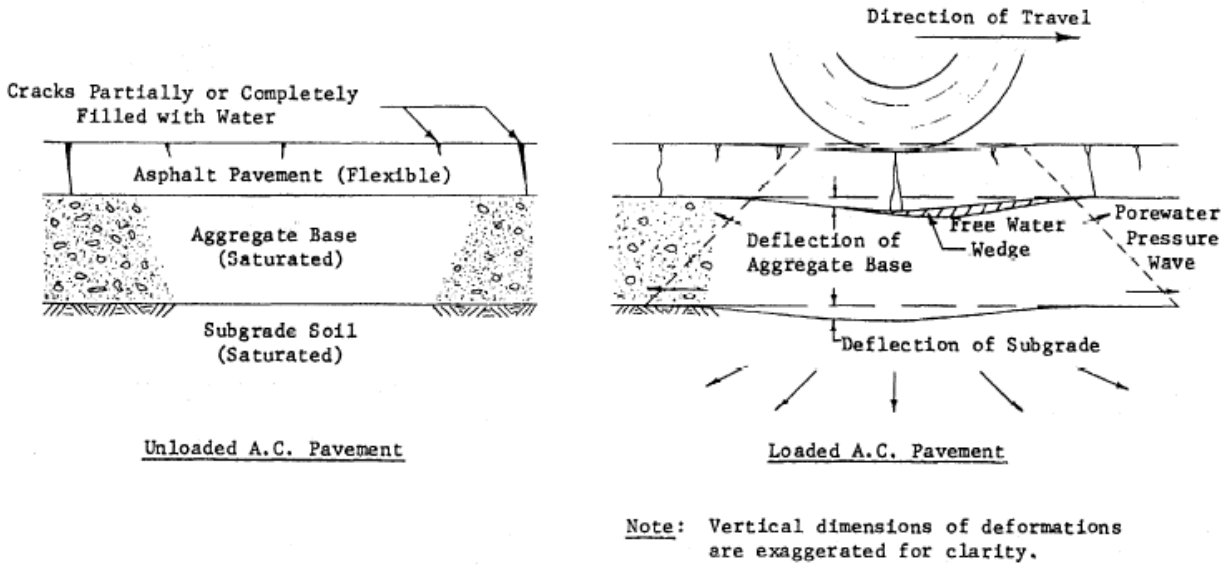

Figure 2.1 Adverse effects of water on asphalt concrete (AC) pavement

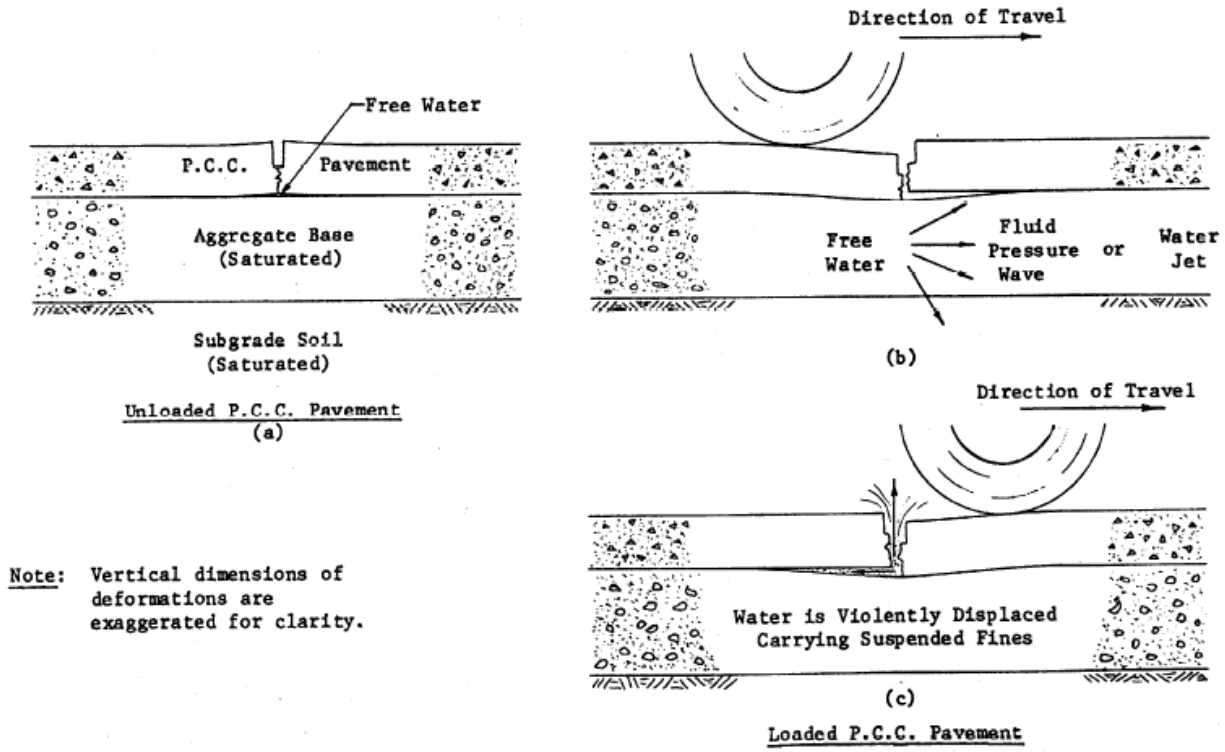

Figure 2.2 Adverse effects of water on Portland cement concrete (PCC) pavement

Another adverse effect of water on pavement structure is called “frost boiling,” which causes extensive damage in northern regions or cold climates. The mechanism of “frost boiling” phenomena is related to frost heave and thaw weakening processes (Chamberlain, 1987), as shown in Figure 2.3. Water drains from coarse-grained base, subbase, and subgrade fairly fast. However, when water encounters courses with more fines, the fine content is susceptible to intrusion into the base layer due to dynamic traffic load, and water migration causes differential settlement. Frost heave is attributed to the formation of ice lenses during freezing. Three key elements are required in ice lens formation: (1) frost-susceptible soils, (2) subfreezing temperature, and (3) available water sources. Frost-susceptible soils (FS) are defined as soils with pore sizes between particles and particle surface areas that promote capillary flow (Casagrande, 1947 and 1987; Csathy and Townsend, 1962). For engineering practice, soils that contain over 10% fines are considered FS soils. During freezing periods, water in large void spaces freezes into ice crystals as the freezing front moves downward. Water expands about 9% by volume and is considered impermeable when frozen. Negative pore water pressure is generated, and ice crystals tend to attract water from adjacent voids. However, frozen soil above the freezing front is impermeable, and the only available water source comes from the unfrozen subgrade beneath the freezing plane. As crystals continue to grow, fed by capillary movement through FS soils, shallow groundwater continuously flows upward to the freezing plane. This causes pavement to heave and sometimes crack. With the arrival of spring, ice lenses start to melt which softens areas within the pavement structure (Taber, 1930 a and b, 1978 and 1980). When water drains out over time, the differential settlement phenomenon can be observed. Soft and weak soils provide limited friction and interlock between subgrade and base materials, resulting in rutting issues.

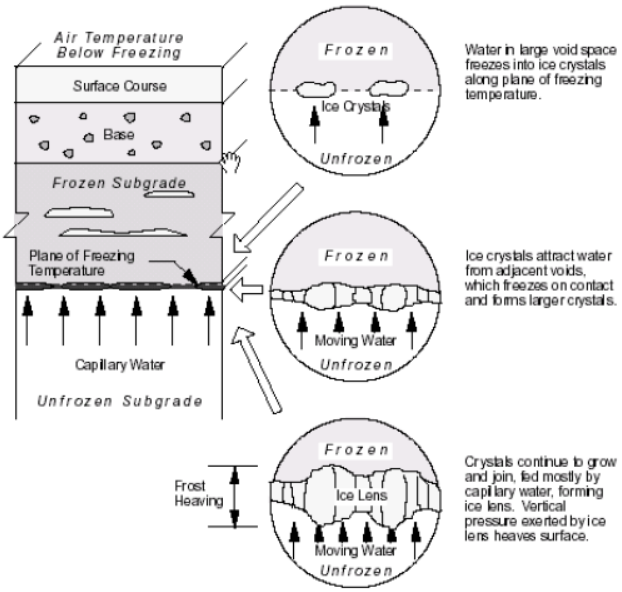

Figure 2.3 Ice lens formation

2.2 Types and Sources of Subsurface Water

Subsurface water exists in four forms: water vapor, bounded water, capillary water and, free (or gravitational) water (Kochina and Ya, 1952; Aravin and Numerov, 1953 and Muskat, 1946). In most cases, water vapor is stored inside soil pores above the saturation zone. In existing subdrainage design methods, water vapor transmission is negligible. Bounded water is relatively hard to move from soil particles and can be considered part of the soil particles. This form of water phase in soil cannot move under gravity force and, therefore, is not considered in most subdrainage design methods. Capillary water is found in soil pores above the saturation zone. However, unlike water vapor, it can flow under the action of surface tension. The height of capillary rise is a function of the size of the soil micro-pores, which relates to soil particle-size distribution and density (Lane and Washburn, 1946; Barber and Sawyer, 1952). Since capillary water does not drain by gravity, the most common way to control capillary water is to lower the water table or use a capillary barrier that blocks the upward capillary flow. The fourth form of subsurface water and the most common type is free water, which is water in liquid form that flows under the force of gravity and obeys Darcy's law. Controlling free water is a major concern in subdrainage design methods.

Subsurface water has a variety of sources and mainly falls into two categories: groundwater and infiltration (Brown et al., 2001). Groundwater refers to water in the saturation zone below the water table. The major source of groundwater is precipitation. Infiltration water is defined as the water that seeps into the pavement structure through pavement surface, shoulders, or median. Precipitation is also the major source of infiltration water. For bituminous pavements, the primary infiltration water source is longitudinal joints at shoulders and construction joints between strips of paving. As for concrete slabs, infiltration water moves through cracks, joints, and shoulders (Cedergren, 1974; Cedergren et al., 1973).

2.3 Conventional Drainage Design Methods

A major design consideration in obtaining sufficient pavement drainage involves the amount of water entering the pavement structure; that is, preventing and quickly removing water that enters the pavement system, using materials that are insensitive to the effect of moisture, and incorporating design methods to minimize water damage (MEPDG, 2004; FHWA, 1980; AASHTO, 1993). One design method used to minimize surface water infiltration is to provide adequate longitudinal and cross slopes. The less time that water is detained on the road surface, the less the infiltration of water into pavements through joints and cracks. Another common method is to seal joints, cracks, and all other discontinuities that allow water to infiltrate into the pavement structure. In addition to the two methods just described, moisture insensitive materials, such as ATB (asphalt-treated base), CTB (cement-treated base), and granular materials with less fines, are popular in controlling the water content of pavement structures.

A subsurface drainage system can be categorized by four types: (1) longitudinal drains, (2) transverse and horizontal drains, (3) drainage blankets, and (4) well systems. A longitudinal drain involves either a trench of substantial depth or a collector pipe (or protective filter) that parallels

the roadway centerline. Transverse drains run laterally beneath the roadway and are designed to drain both groundwater and infiltration water in base and subbase courses. Drainage blankets refer to a very permeable layer that can be used beneath or as an integral part of the pavement structure to remove infiltration water or groundwater from both gravity and artesian sources. Although base and subbase courses are relatively permeable, they are not considered drainage blanket layers unless they are specially designed with a high coefficient of permeability, have a positive outlet for water collection, and have a protective filter layer. A system of vertical wells has been used to lower the groundwater level and relieve pore water pressure. Sand-filled vertical wells are commonly used to accelerate the drainage of soft and compressible foundation materials (Rutledge and Johnson, 1958; Rechart, 1957).

In recognition of the impact that moisture can have on pavement performance, the AASHTO Design Guide (AASHTO, 1993) incorporated an empirical drainage coefficient into design equations. The following are three approaches commonly employed to control or reduce moisture problems:

1. Prevent moisture from entering the pavement system. Provide adequate cross slopes and longitudinal slopes. In general, the less time that water stays on the pavement slopes, based on the pavement surface, the less moisture can infiltrate through joints and cracks. (Anderson et al., 1998). Joint and crack sealing is required throughout the pavement service life.
2. Use materials that are insensitive to the effects of moisture, such as lean concrete base, cement-treated base, asphalt-treated base, and gravel base with limited fines. Open-graded material allows easier movement of moisture through material.
3. Remove free water through subsurface drainage. Consider providing three types of drainage systems: surface drainage, groundwater drainage, and subsurface drainage (subdrainage). These three drainage systems are only effective with free water. Water held by capillary forces in soils and in fine aggregates cannot be drained. The effects of this bound moisture are considered in the EICM (Enhanced Integrated Climate Model) through adjustments to pavement materials properties.

The Mechanistic-Empirical Design Guide (FHWA, 2004) is the most commonly used pavement design guidebook. Within Appendix SS of the guidebook, a comprehensive description of a drainage design method is introduced. The method compares inflow and drainage capacity to determine if a drainage design is sufficient for draining both groundwater and infiltration water quickly enough.

2.3.1 Estimation of Inflow

Water inflow sources include surface infiltration, groundwater infiltration, and meltwater (from ice lenses). Surface infiltration is the most important water inflow source and should always be considered in a subdrainage design. Groundwater should be lowered by deep longitudinal drains and should not be allowed to seep into the pavement structure. If this is not feasible, the amount of seepage entering the drainage layer should be estimated. Meltwater from ice lenses only needs

to be considered in northern climates where frost heaves occur. Because fine-grained soils are impermeable, it is unlikely that flow from both groundwater and meltwater will occur at the same time. Therefore, only the larger of the inflows needs to be considered.

The amount of infiltration is related directly to cracking. For evaluating the amount of water via infiltration, the duration of rainfall is a more critical factor than the intensity. Equation 1 is adopted to determine the infiltration rate and Figure 2.4 shows the isotropic precipitation rate contour.

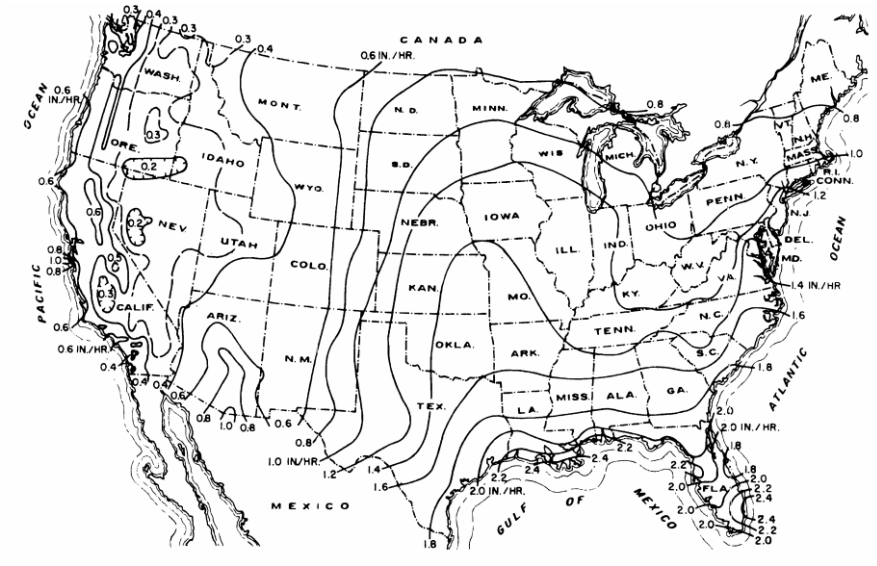

Figure 2.4 1-hour/1-year precipitation rate

$$q_i = I_c \left(\frac{N_c}{W_p} + \frac{W_c}{W_p C_s} \right) + k_p \tag{1}$$

where
q_i = infiltration rate per unit area, $ft^3/hr/ft^2$
I_c = cracking infiltration rate, 2.4 $ft^3/day/ft$
N_c = number of longitudinal cracks
W_p = width of pavement subjected to infiltration
W_c = length of transverse cracks or joints
C_s = spacing of transverse cracks or joints
k_p = rate of infiltration through uncracked pavement surface, which is usually equal to the coefficient of permeability of HMA or PCC.

By assuming that $N_c = N + 1$, (N is number of traffic lanes), $W_c = W_p$, $k_p = 0$, infiltration rate is 0.1 $ft^3/day/ft$ of crack, the inflow rate can be written as

$$q = q_i W_p = 0.1\left(N + 1 + \frac{W_p}{C_s}\right) \quad (2)$$

As for groundwater seepage, assuming that the pavement bottom is an impermeable layer, the inflow is divided into two parts: inflow above the bottom of the drainage layer, q_1, and inflow below the drainage layer, q_2. The drainage layer is used to lower the water table, in addition to providing drainage for surface infiltration.

$$q_1 = \frac{k(H-H_0)^2}{2L_i} \quad (3)$$

where
q_1 = volume of flow per unit time per unit length of the longitudinal drain, $ft^3/day/ft$
k = permeability of the subgrade soil
H = initial height of the groundwater table above the impervious layer
H_0 = vertical distance between the bottom of drainage layer and the impervious layer
L_i = distance of influence, $L_i = 3.8\ (H-H_0)$.

After q_1 has been determined, use the chart in Figure 2.5 to determine q_2. The lateral or horizontal flow is

$$q_L = q_1 + q_2 \quad (4)$$

The groundwater inflow to the drainage layer per unit area is

$$q_g = \frac{2q_2}{W} \quad (5)$$

where
W = width of the roadway.

However, if the pavement is sloped to one side and the collector pipes are installed only on one side, the lateral flow per unit length of pipe is

$$q_L = 2(q_1 + q_2) \quad (6)$$

$$q_g = \frac{q_1+2q_2}{W} \quad (7)$$

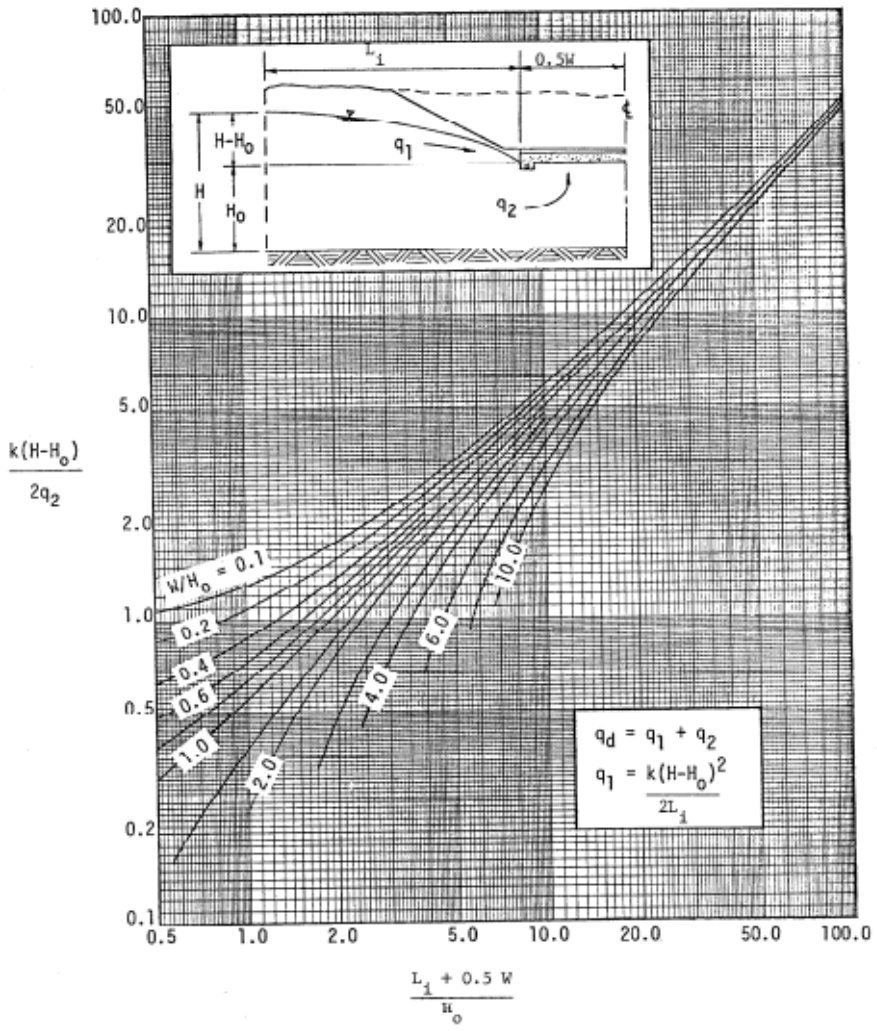

Figure 2.5 Flow rate in horizontal drainage blanket

The design inflow is the sum of inflows from all sources minus the outflow through the subgrade soil. When the subgrade is not affected by any water table, a simple and conservative method is to assume the hydraulic gradient to be 1, so the outflow rate is equal to the permeability of the soil. The outflow through subgrade depends on the permeability of the soil and on the water table at the boundary and can be determined by the use of a flownet or another simplified design chart. If the outflow through the subgrade is neglected, the design inflow can be determined by one of the following combinations:

1. If there is no frost action, the design inflow, q_d, is the sum of surface infiltration q_i and groundwater flow q_g:

$$q_d = q_i + q_g \tag{8}$$

2. If there is frost action, q_d is the sum of surface infiltration qi and inflow from meltwater q_m:

$$q_d = q_i + q_m \tag{9}$$

2.3.2 Estimate Drainage Capacity

There are two design requirements for a drainage layer: (1) the steady-state capacity must be greater than the inflow rate, and (2) the unsteady-state capacity must be such that the water can be drained quickly after each precipitation event. Discharge is composed of two parts: discharge through area, *H*, caused by the hydraulic gradient, *S*; or through area *H*/2, caused by the hydraulic gradient *H/L*. When $S = 0$, $q = 0.5\text{kH}^2/\text{L}$, which is a direct application of Darcy's law, assuming that the surface is at the top of the drainage layer on one end and at the bottom of the layer on the other end, which is an average flow area of *H*/2.

For steady-state flow:

$$q = kH(S + \frac{H}{2L}) \tag{10}$$

where
q = discharge capacity of the drainage layer
k = permeability of the drainage layer
S = slope of the drainage layer
H = thickness of the drainage layer
L = length of the drainage layer.

For unsteady-state flow:

Unsteady-state flow capacity is defined by the degree of drainage, which is a ratio between the volume of water drained since the rain stopped and the total storage capacity of the drainage layer. The time for a 50% degree of drainage can be computed as follows:

$$t_{50} = \frac{n_e L^2}{2k(H+SL)} \tag{11}$$

where
t_{50} = time for 50% drainage
n_e = effective porosity, which is the porosity occupied by the drainage water.

For excellent drainage, AASHTO (1993) requires that the water be removed within 2 hours. For design of the drainage layer, the requirement that the time for complete or 95% drainage be less than 1 hour appears to be more appropriate. The degree of drainage, *U*, depends on a time factor T_f, and a slope factor, S_f, respectively, defined as

$$T_f = \frac{kHt}{n_e L^2} \tag{12}$$

$$S_f = \frac{LS}{H} \tag{13}$$

2.4 Comparisons of Conventional and New Drainage Design Concepts

In investigating existing pavement drainage design methods and criteria (MEPDG, AI, Shell, and ASSHTO), we found that they only address "free water" or gravitational water flow, and that water detained by capillary force or in fine soils (in unsaturated conditions) cannot be drained. When a pavement structure is built, it is often built with soils at their optimum moisture contents to achieve the best performance. After construction, surface soils are exposed to the surrounding atmospheric environment and dry quickly, since the relative humidity in the air is often less than 90%. Such relative humidity corresponds to a suction value of 140 MPa (Fredlund and Rahardjo, 1993). All soils become air-dried under such high suction. Air enters the voids in the soils, and the surface soils form a dried crust that has very low permeability (nearly impermeable) to transport water from inside to outside. In the meantime, the soils inside the pavement structure tend to reach equilibrium with the surroundings (normally the groundwater table) through capillary rise, as shown in Figure 2.6.

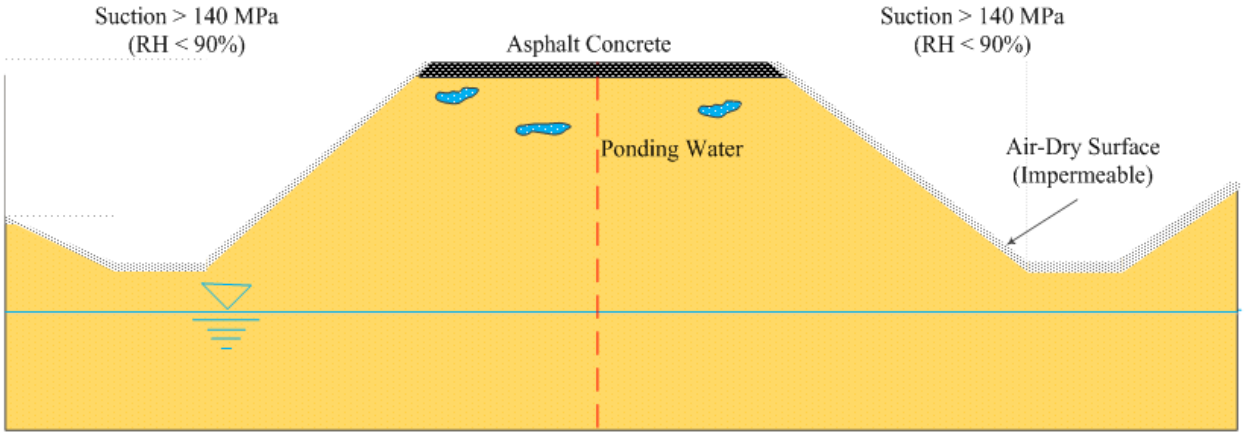

Figure 2.6 Conventional drainage design concept

When surface soils air-dry and have cracks, they are highly permeable for water infiltration. Infiltrated water ponds in the upper part of pavement in unsaturated conditions lead to low suction. Other factors such as water vapor condensation below the pavement surface during decreased nighttime temperatures can also lead to water content increase in base and subbase materials. The pore water pressure in soils is negative when soils are unsaturated. Hence, water cannot be drained by a conventional drainage system, which is typically made of granular material with large voids and relies on gravity as a driving force for drainage. Instead, air easily enters the large voids and blocks outward liquid water flow. Although granular materials are sometimes used as a capillary barrier for liquid water flow to mitigate frost heave and thaw-weakening problems, they cannot prevent water flow in vapor form inside the embankment. Over time, the moisture content of soils

in the pavement embankment will increase, even if there is a granular drainage layer. Another common way to deal with water drainage is to use geosynthetics as capillary barriers to prevent capillary flow. Geosynthetics can act as capillary barriers because the suction in fine-grained soils prevents water flow to larger geotextile pores. However, suction decreases incrementally in water content. When suction decreases to the air entry value, the geotextile ceases as a capillary barrier. Meanwhile, the accumulated water in the overlying soils weakens the granular base or subbase layers due to additional stored moisture. This situation could cause a problem with geotextiles, geonets, and geocomposites in unsaturated conditions.

In contrast, see Figure 2.7 for a new conceptual design. The installation of a layer of wicking fabric in the base layer parallel to the pavement surface is proposed. At the two shoulders of the embankment, the wicking fabric is exposed to the atmosphere with a length of 2–3 meters. Due to its hydrophilic and hygroscopic nature, the wicking fibers can absorb water from the surrounding soils inside the embankment. As discussed previously, there is big difference in the relative humidity or suctions between the soils inside the embankment and the atmosphere. This difference in relative humidity provides the driving force for the wicking fabric to draw water out of the pavement structure to the embankment shoulder, where the water is vaporized in the air to reach an equilibrium condition. Unlike the conventional granular or geotextile drainage system, wicking fiber contains many microchannels that can maintain saturation under low relative humidity (or high suction value). Consequently, the wicking fabric builds a liquid connection between the inside and the outside of the pavement structure for continuous water removal. Compared with the amount of water needed to saturate Earth's atmosphere, the amount of water in the embankment is miniscule. Therefore, the wicking process will continue until air enters the microchannels of the wicking fibers.

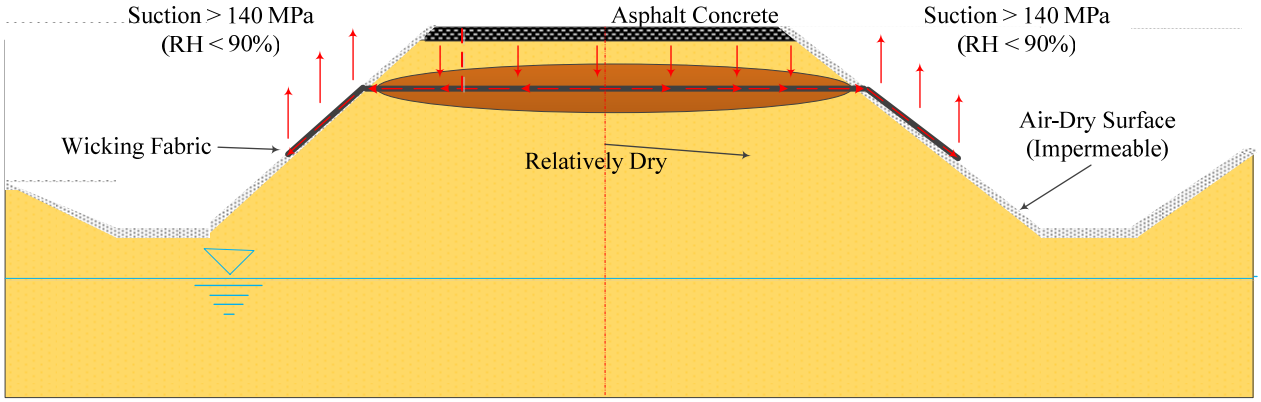

Figure 2.7 New drainage design concept

2.5 Geosynthetic Application in New Drainage Design

Geosynthetics are synthetic and polymeric materials used in civil engineering. There are eight major product categories: geotextile, geogrid, geocell, geomembrane, geofiber, geofoam, geosynthetic clay liner, and geocomposite (see Figure 2.8). Geosynthetics have a wide range of

applications in geotechnical engineering, such as for roads, airfields, embankments, retaining structures, and reservoirs.

Figure 2.8 Geosynthetic categories

Geotextiles and geogrids are the two types of geosynthetics most commonly used in the geotechnical engineering field. The major geosynthetic functions for roadway stabilization and reinforcement are separation, confinement, soil reinforcement, filtration, and drainage. Geotextiles can be used as separation material, placed between two dissimilar materials to maintain the integrity of both materials. For confinement function, geotextiles and geogrids can be used to prevent the aggregate lateral movement that compromises roadway and pavement structure performance. Geotextiles take advantage of friction, while geogrids use interlock to mitigate relative movement. For reinforcement function, both geotextiles and geogrids work effectively to spread the load and prevent excess load on different components that form the road.

Even though geotextiles provide separation, confinement, and reinforcement functions, when it comes to filtration and drainage function, geotextiles definitely show more advantages than geogrids. Geotextiles allow free water to flow across the geotextile plane while controlling soil particle retention. As water and small particles drain through confined layers of aggregates and

subgrade, smaller particles are eventually trapped between bigger ones, which results in larger grading and provides a more stable layer. It is impossible to filter aggregates by using geogrids because geogrids have much larger openings.

2.6 Geotextile with Wicking Ability

Recently, a geotextile with lateral drainage function was developed. This material has potential for use in reducing the water content within road and pavement structures (see Figure 2.9[a]). This type of geotextile is a dual-function product that contains a high modulus polypropylene yarn for reinforcement and stabilization. The double woven layer construction provides excellent separation and filtration functions. The uniform openings provide consistent filtration and flow characters for fine to coarse sand layers. The double layer design can provide effective confinement between base and subbase materials, resulting in greater load distribution and good durability performance. Unlike traditional geotextiles, this new material includes special hydrophilic and hygroscopic 4DG^{TM} fibers that provide wicking action through the plane of the geotextile (Figure 2.9[b]). The deeply grooved cross section (Figure 2.9[c–d]) provides a larger surface area, thus ensuring that the channel holds and transfers larger amounts of water even in unsaturated conditions. The average diameter of the wicking fabric is between 30 and 50 μm, and the average groove spacing is between 5 and 12 μm. Detailed information on geotextile hydraulic and mechanical specifications can be found in Table 2.1. When properly designed, geotextiles have the potential to dehydrate the subgrade and base course under unsaturated conditions and, consequently, to improve the performance of pavements.

TenCate Geosynthetics performed preliminary tests (see results in Table 2.1). The innovative geotextile could transport water a distance of 72 inches (within 16.5 hours) with zero gradient in drainage tests (as shown in Figure 2.10[a]) and wick water to a height of 10 inches (within 2 hours) during capillary rise testing (Figure 2.10[b]). The horizontal and vertical wicking tests were conducted at room temperature with relative humidity less than 40%, which indicates that the geotextile can successfully transport water under unsaturated conditions. The horizontal wicking test proved that the geotextile can transport water without hydraulic gradient, and the vertical wicking test further validated that capillary force was greater than gravity and could draw water to a depth of 10 inches. Neither test measured the amount of water evaporated. It is expected that the actual wicking distance and/or height are longer and higher than the test results indicate.

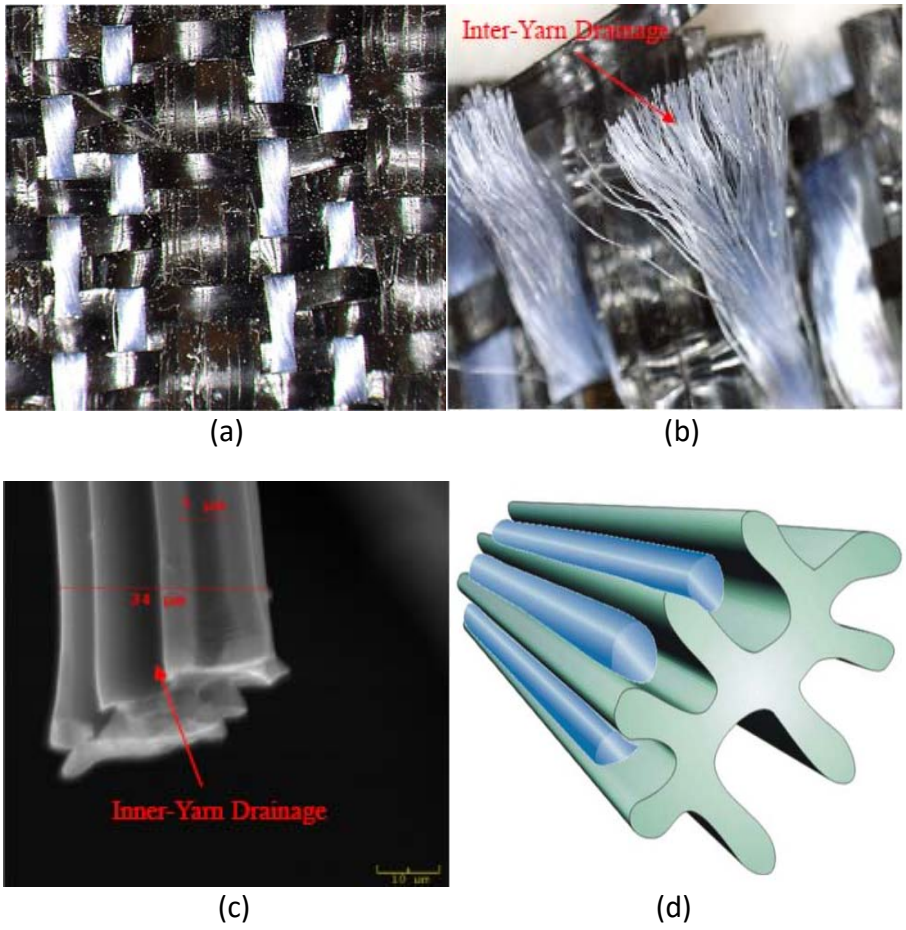

Figure 2.9 Innovative geotextile with wicking fabric

Table 2.1 Geotextile specifications

Mechanical Properties	**Test Method**	**Unit**	**Average Roll Value**
Tensile Modulus @ 2% Strain (CD)	ASTM D4595	kN/m	657
Permittivity	ASTM D4491	Sec^{-1}	0.24
Flow Rate	ASTM D4491	$l/min/m^2$	611
Pore Size (050)	ASTM D6767	Microns	85
Pore Size (095)	ASTM D6767	microns	195
Apparent Opening Size (AOS)	ASTM D4751	mm	0.43
			Tested Value
Wet Front Movement (24 minutes)	ASTM C1559	inches	6.0 Vertical Direction
Wet Front Movement (983 minutes) Zero Gradient	ASTM C1559	inches	73.3 Horizontal Direction

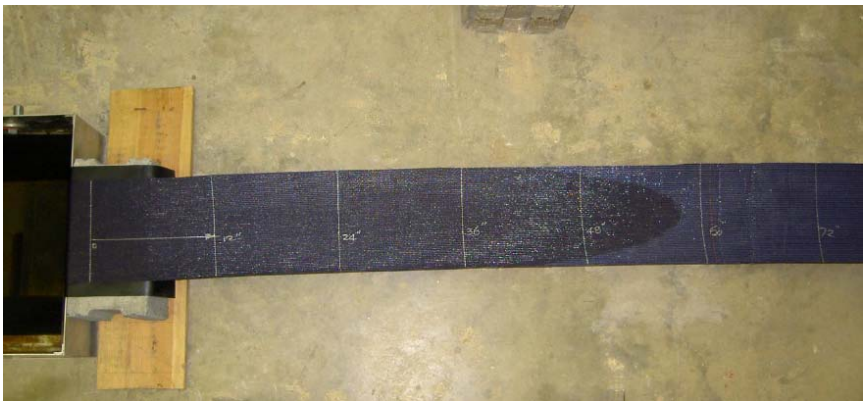

Horizontal Wicking Length Test

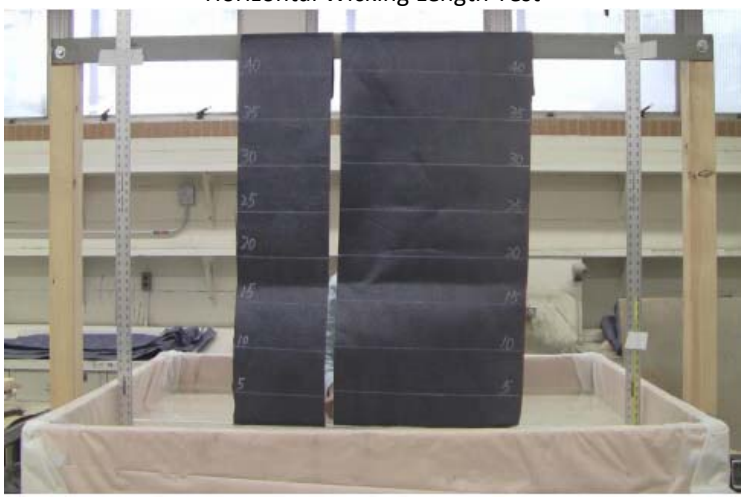

Vertical Wicking Height Test

Figure 2.10 Wetting front movement tests

Researchers at the University of Alaska Fairbanks (Zhang and Belmont, 2010) conducted a series of tests with geotextiles, including drainage, capillary rise, rainfall infiltration, and frost heave tests, to evaluate the effectiveness of the material in controlling frost heaves. The researchers found that the material's vertical wicking height was 12 inches, which was slightly different from TenCate's results. The variation might have been the result of several factors, such as temperature, relative humidity, and testing width of the geotextile. As for the rainfall infiltration test, the testing apparatus is shown in Figure 2.11. Four different types of geotextile were used in the rainfall infiltration test, including a wicking fabric, a high performance (HP) reinforcement geosynthetic, a geotextile water filter, and a drainage composite. The test soil was first saturated and compacted within a plastic mold. Then the mold was put upside down on a layer of geotextile with an impermeable membrane beneath it. The water was allowed to flow for 3 days. Test results indicated that conventional geosynthetics, woven and non-woven, ceased to transport water within 1 day. This phenomenon could be explained by the relatively low air entry values of the geosynthetics. Due to the larger pore size of the geosynthetic, air could easily block the voids under low suction value. Air bubbles were considered similar to soil solids, which were impermeable to water flow. However, the atmospheric suction value could be as high as 140 MPa, and the

geosynthetics could be dried fast under room temperature and relative humidity. Therefore, within a limited time, the geosynthetics ceased to transport water, and the test soils would have larger final water content. In contrast, the geotextile with wicking fabric had a large surface area and large air entry value, which enabled the geotextile to wick water out of the soil under higher suction value and resulted in a lower final water content, as shown in Figure 2.12. Test results of the four different types of geotextile further confirm that the geotextile has advantages at wicking water out of soil under unsaturated conditions.

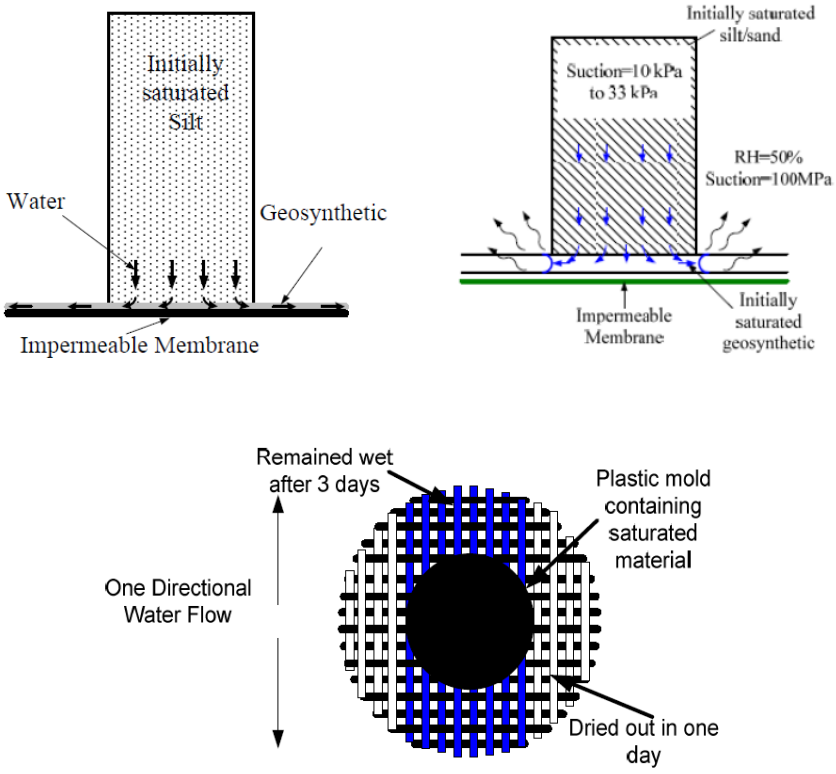

Figure 2.11 Schematic plots of rainfall infiltration test

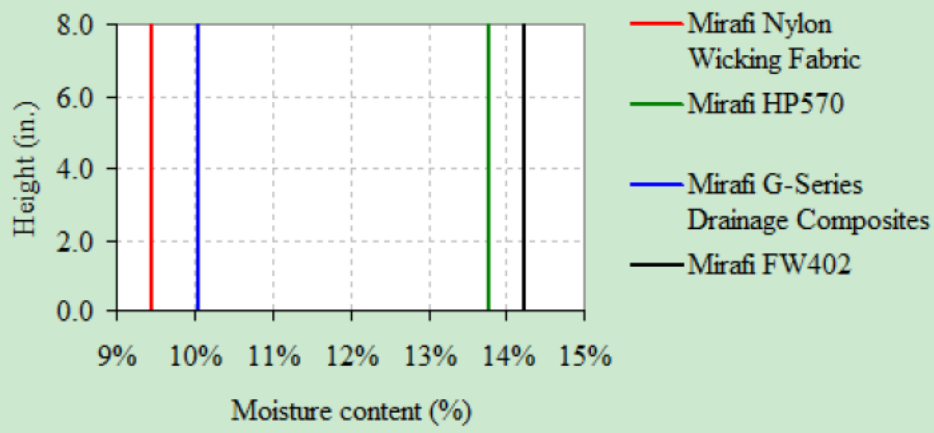

Figure 2.12 Rainfall infiltration test results

Wang et al. (2015) also evaluated the effectiveness of geotextile wicking ability under unsaturated and rainfall conditions. To simulate field conditions, the researchers sandwiched a layer of the innovative geotextile with a 152 mm thick AB3 subgrade and a 381 mm thick subgrade that was mixed with Kansas River sand and kaolinite. The geotextile extended out of the closed system to the dehumidifier section so that water could be wicked out. Water in the amount of 11.3 kg was poured into the system to simulate a 38.1 mm/hour rainfall, and the water contents with depths were monitored. Test results indicated that the geotextile effectively wicked water out of soils compacted at optimum moisture content, and the water wicked out by the geotextile was 1.65 times greater than the water transported by gravity. Therefore, lab test results provide strong evidence that this type of geotextile has the potential to wick water out of soils under unsaturated conditions and is competitive compared with other types of geotextiles.

2.7 Case Studies of Geotextile with Wicking Ability

Although both laboratory test results indicated that H2Ri is a promising drainage material for wicking water out of pavement structure, no direct evidence was available to prove its good field performance. In addition, there were some concerns that smaller soil particles would block the innovative geotextile material and that a mechanical puncture would cause malfunction. In addition to the information gleaned from lab tests, several reports and papers were found regarding the wicking performance of the innovative geotextile as discussed in the following cases.

Case 1: Beaver Slide, Alaska

Zhang et al. (2014) reported successful application of the innovative geotextile material to prevent frost boils in Alaska pavements. Their project was located at a section of the Dalton Highway named Beaver Slide, an unpaved roadway with significant heavy truck traffic. Frost heave and thaw weakening had caused extensive damage to the pavement structures. Previous rehabilitation using geocomposites had proved unsuccessful. In total, 22 TDR sensors were used to monitor the temperature and water content change of a 60-foot-long road section, the softest spot, as shown in Figure 2.13. Sieve analysis results indicated that some soils had fines content

larger than 6%, which is considered frost-susceptible (FS) soils. Two layers of H2Ri geotextile were installed 45 cm apart with the bottom layer geotextile. In addition to the temperature and water content sensors inside the test section, other sensors recorded useful data on air temperature and relative humidity for over 2 years.

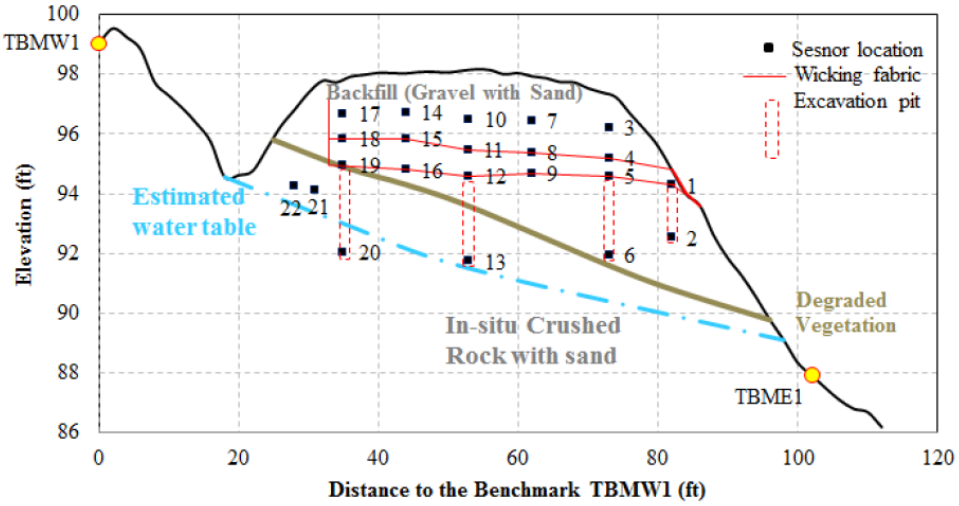

Figure 2.13 Schematic plot of test section

Performance of the geotextile was monitored under different climate conditions, such as rainfall events, the freezing process, and the thawing process. During a rainfall event (Figure 2.14[a]), the water penetrated to a depth of 3 feet below the road surface. The drying process proceeded from east to west, which was exactly the geotextile drainage direction. A drier zone between the two geotextile layers also indicated that the geotextile had greater permeability than the surrounding unsaturated soils and enabled faster drainage. For the freezing process (Figure 2.14[b]), the freezing front penetrated to a depth of 6.5 feet at the beginning of November 2010 and continued to penetrate downward to the bottom of the roadway. The unfrozen water content was less than 10% after the roadway was completely frozen. As for the thawing process (Figure 2.14[c]), even though the water content was expected to increase, the soil did not reach saturation during spring thaw.

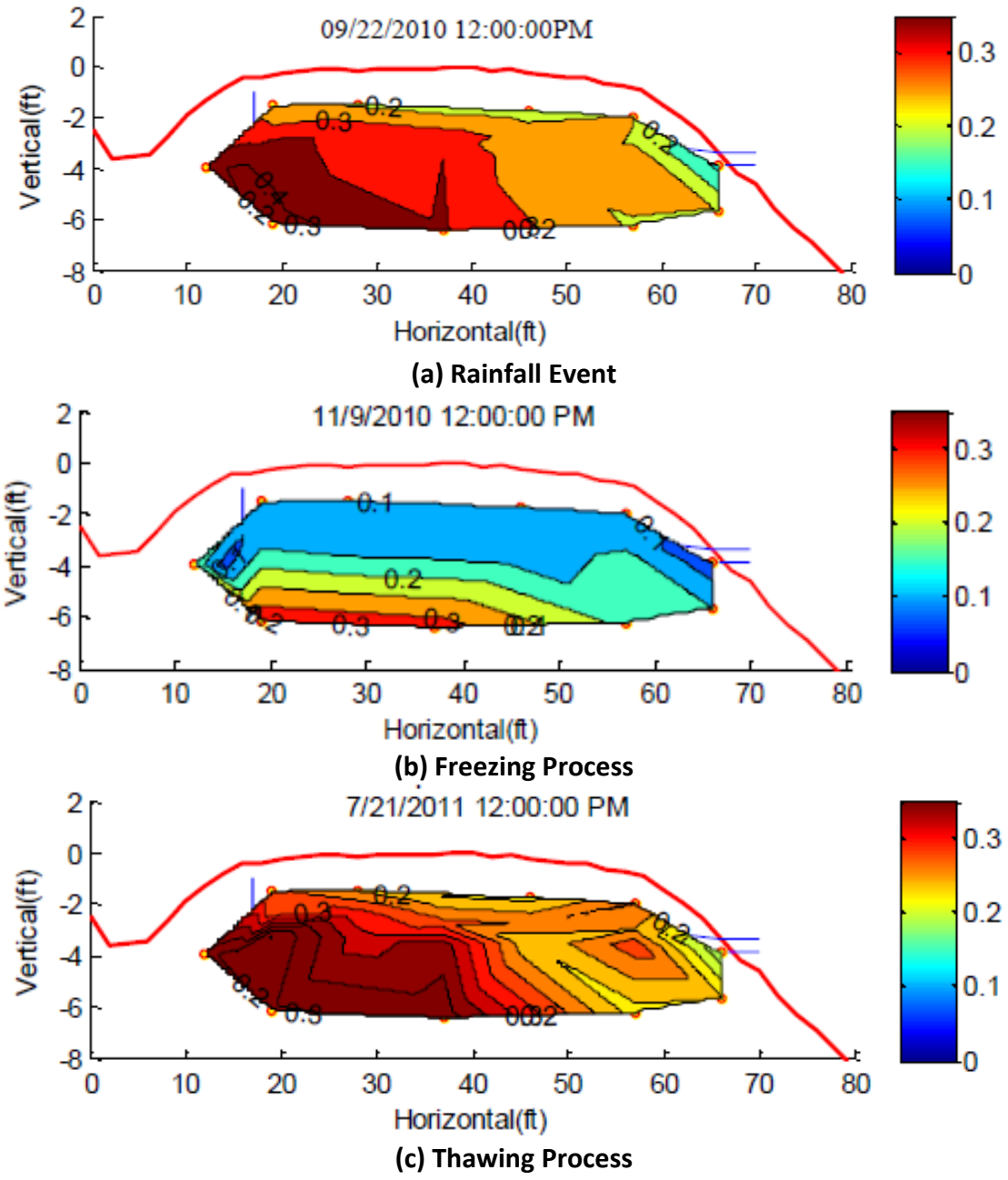

Figure 2.14 Moisture contours in the test section

In summary, over 2 years of monitoring shows good overall performance of the testing section. Field observation clearly showed a road surface difference between sections with and without geotextile, as shown in Figure 2.15. No soft spots have been observed during early springs, and soil at the shoulders is damp, which indicates that water flows along the direction of the geotextile wicking fabric. The geotextile successfully eliminated weakening of the structural section due to excess water during the spring. Even though soil 4.5 feet beneath the surface and lower showed the existence of excess water, the soil at that point is beyond the depth of frost heave and thaw

weakening and had limited effect on roadway performance. It is clear that the H2Ri significantly reduced the flow of water to the surface during the fall months eliminating excess water in the structural layer during the freezing process. This is particularly impressive since the fall is the wettest season in this area.

Figure 2.15 Test section comparison

Case 2: Coldfoot, Alaska

Frost heave problems similar to Beaver Slide occurred in a harsh environment about 30 miles north of Coldfoot, Alaska. The road is located in an area of extremely cold winter temperatures. A 12-mile test section (6 miles with geotextile material and 6 miles without) was constructed in 2012 in an effort to mitigate the frost heaving and prevent ice lens formation. Twelve inches of aggregate over the geotextile was completed on one lane first. Then the other lane was constructed using the same structure with a minimum of 1.5 feet of geotextile overlap. The goal was to reduce the weakening of the upper 1.5 feet of material which carries 80% of the load. Test results showed successful application of the geotextile to stop water from rising to the subgrade via capillary action. Since this project is new, close monitoring is required to evaluate overall long-term roadway performance. However, as shown in Figure 2.16, preliminary observations indicate that the geotextile material has effectively served as a capillary break, wicking water out of the structural section.

Figure 2.16 Preliminary field observation at Coldfoot, Alaska

Case 3: St. Louis County, Missouri

In this case, a new bridge was being constructed over the Missouri River. The objective in using the geotextile material was to remove water from underneath the pavement section. The original design was to construct a pavement section with 4 inches of base aggregate, 4 inches of drainable aggregate, and a prepared subgrade. It was expected that the geotextile could reduce the aggregate base material by 2 inches, and wick water from under the pavement. Observation is shown in Figure 2.17. The results proved that the geotextile successfully wicked water out of the aggregate.

Figure 2.17 Field observation at St. Louis County, Missouri

Case 4: Texas County, Texas

Zornberg et al. (2013) discuss several cases involving innovative geotextile material in pavement construction and rehabilitation projects. One of the applications was the Texas State Highway 21 rehabilitation project to control different settlement in expansive clay subgrades. The testing area included eight sections with four different types of separator geotextiles, as shown in Figure 2.18. Unfortunately, no conclusive results indicate the effectiveness of the innovative geotextile to change the water content in subgrades. This might be because of the high plasticity of the subgrade soil (Plasticity Index = 35%). Another case mentioned in this paper is in Lecheria, Mexico, where a pavement section was constructed over a high plasticity clay embankment. A wicking fabric geotextile was used in this project to reduce differential settlement of the plastic clay by balancing non-uniform distribution of moisture, and to reinforce the base course of the road section. Wicking fabric geotextile was placed on top of the subgrade soil to reduce the vertical flow of water and dissipate it in the horizontal direction. The geotextile was also designed to reinforce the base layer so that the base layer thickness would be a minimum of 38 cm (15 inches). The performance of these sections is currently being monitored.

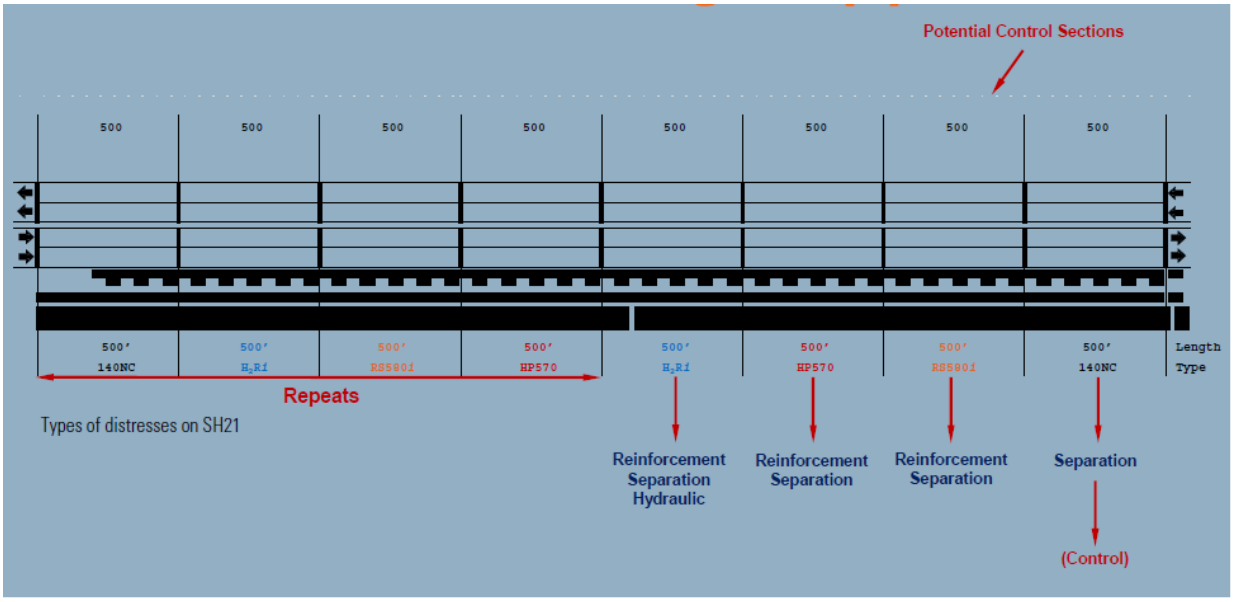

Figure 2.18 Schematic plot of test section at Texas County, Texas

Case 5: Corona, California

In Corona, California, a large section of roadway had become saturated by an excessive amount of natural water run-off, causing the roadway section to fail. The geotextile with wicking fabric was used to help drain away the excess water while providing enhanced stabilization (Figure 2.19). A 6-inch layer of base material was placed on top of the geotextile. A layer of geogrid was placed on top of that, followed by another 6-inch layer of base material. A 4-inch layer of AC was the final element of design to complete the road section. Observation indicated that the geotextile provided superior tensile strength at low strain for subgrade support, separated the natural subgrade

soils from the aggregate base, wicked excess water, and provided lateral confinement for the base section.

Figure 2.19 Field construction at Corona, California

Case 6: Jefferson County, Wisconsin

Another application of geotextiles occurred at Jefferson County, Wisconsin, where the material was used to solve a differential settlement problem. The primary challenge was the presence of wet and saturated silt and peat deposits to depths exceeding 30 feet below the existing pavement. Simply removing the deposits was not an economically feasible solution. The geotextile was directly placed on the exposed subgrade, followed by a 15-inch lift of crushed stone, a single layer of geogrid, and a 15-inch lift of crushed stone, as shown in Figure 2.20. The Jefferson County Highway Department reported that subgrade undercutting was minimized to 30 inches, compared with a potential 5–8 feet undercut (or more) for the soil conditions present. In addition to the cost savings, a substantial time savings was realized in the project construction schedule.

Figure 2.20 Field construction at Jefferson County, Wisconsin

2.8 Potential Issues

Although laboratory and field test results indicated the promise of wicking fabric for road uses, concerns remained over the use of wicking fabric for more general conditions. After all, the overall performance of geosynthetic-reinforced pavement structure is dependent not only on the geosynthetic, but also on the soil and soil–geotextile interaction. Before extensive engineering applications of this type of geotextile, several issues need consideration. For example, can the application of wicking fabric be extended to other types of soils? To what extent can the pavement structure water content be reduced? By implementing this type of wicking fabric, how much improvement can be expected for the pavement structure in terms of resilient modulus, permanent deformation, and shear strength along the soil-wicking geosynthetic interface? Most importantly, will the wicking fabric stop working? If so, in what conditions?

Besides these considerations, there are some other concerns regarding geotextile applications. Figure 2.21 shows scanning electron microscope (SEM) images of samples collected from the field. Figure 2.21(a) shows a SEM image of wicking fabric at the surface of the woven geotextile. The "clogging effect" is defined as (1) the magnitude of confining pressure in soil on the drainage path, (2) a physical disturbance on the drainage path, (3) air bubbles stuck in the drainage path, and (4) permeability influenced by the intrusion of fine particles (Palmeria and Gardoni, 2000). Observed results indicate that all surface edges of the wicking fabric were affected by clogging. Since the soil above the geotextile was consolidated, the soil thoroughly blocked the wicking path (soil was detained on the deep grooves) and impeded drainage efficiency. However, in contrast, Figure 2.21(b) shows the SEM images of wicking fabrics beneath the surface. The drainage paths were clean, and a limited amount of soil particles was detained within the drainage paths. Therefore, the clogging effect only occurred at the geotextile surface, and its effect on geotextile performance needed further investigation. One recommendation to minimize clogging effect might be to twist the wicking fabric yarn during the fabrication process to reduce the surface exposed to the soil.

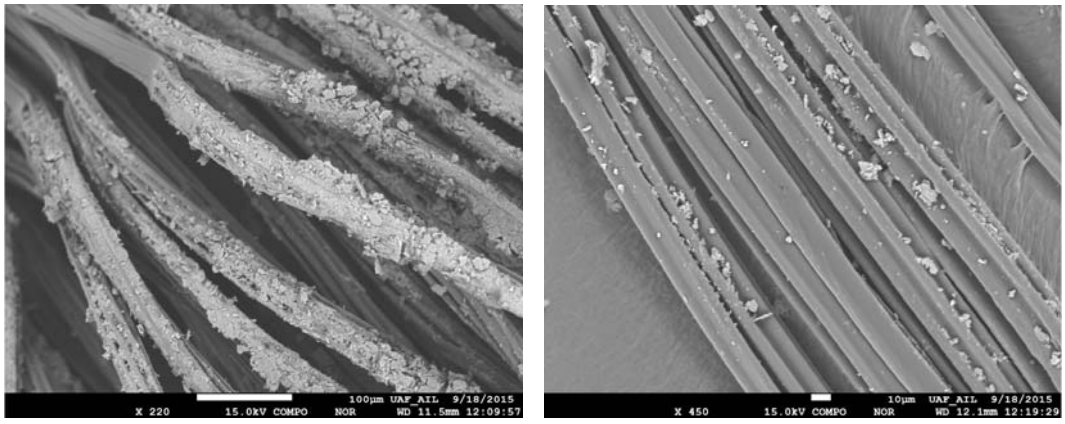

(a) (b)

Figure 2.21 Clogging effect SEM images

Figure 2.22 shows another potential wicking fabric failure due to high vertical pressure. The woven part of the fabric was compressed, and all wicking paths were squeezed together. Figure 2.22(a) shows the fabric yarn without disturbance. Again, all surface layers exposed to soil were affected by clogging, while the overlapped wicking fabrics were mechanically compressed by higher vertical pressure. A closer top view of the compressed area is shown in Figure 2.22(b). The drainage paths were flattened and might not hold and transport water through the grooves. Even though no soil particles were detained here, the deep groove may fail to work under unsaturated conditions, which would compromise draining efficiency. Figure 2.22(c–d) show the compressed area from different angles. Since vertical pressure was much larger than confining pressure, the deep grooves were only compressed in one direction, which means the grooves in the confining direction might still work.

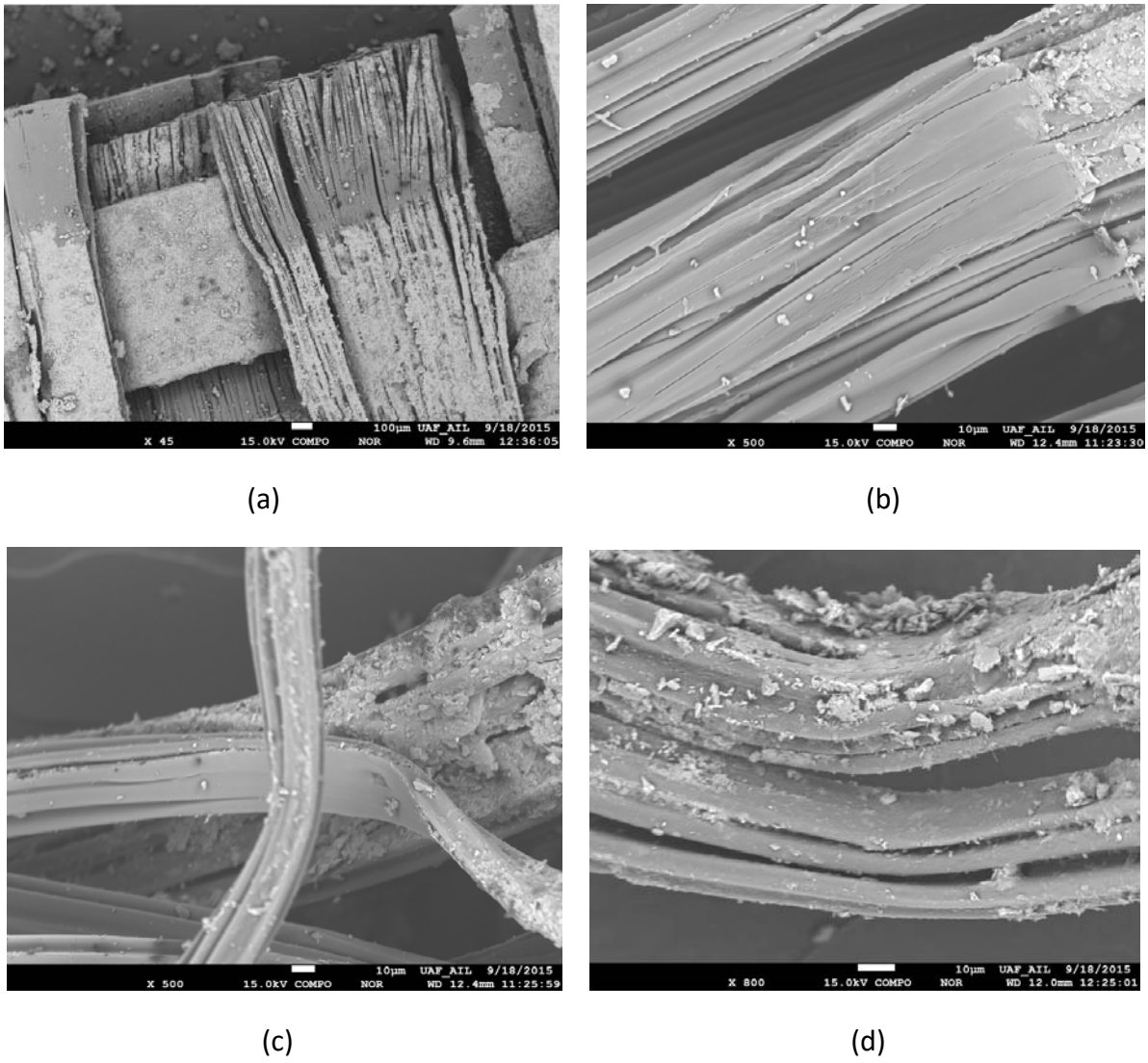

(a) (b)

(c) (d)

Figure 2.22 Mechanical failure SEM images

Figure 2.23(a–b) show wicking fabric failure due to puncture. Although the wicking fabric is strong, puncture failure under high pressure would cause the worst scenario, since the deep grooves are entirely broken off and the drainage paths are thoroughly discontinued.

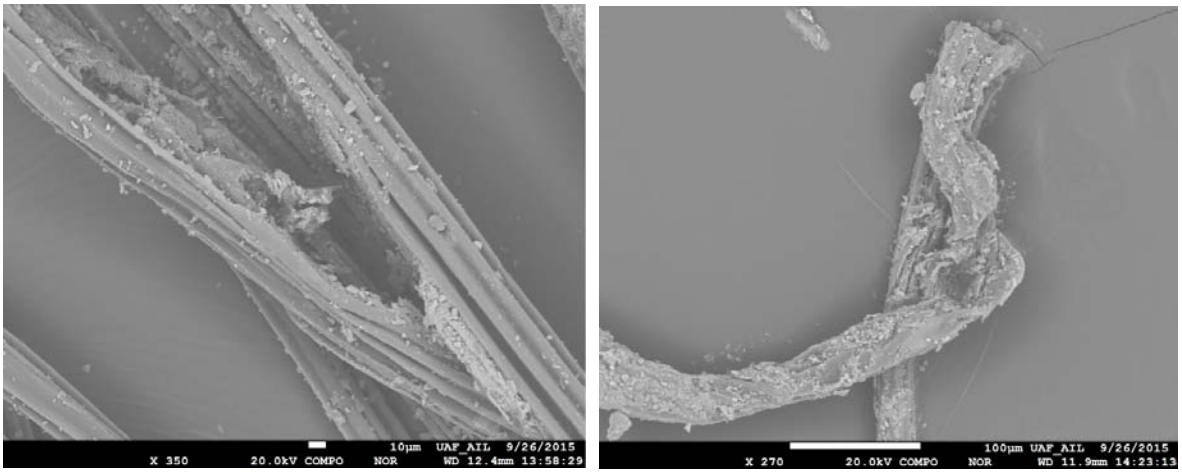

(a) (b)

Figure 2.23 SEM images of puncture failure

CHAPTER 3 RELATIONSHIP BETWEEN SOIL SUCTION AND H2RI PERFORMANCE

The soil water characteristic curve (SWCC) defines the relationship between water content and suction. By understanding the SWCC of both the wicking fabric and the soil, one can assess the potential benefits of the wicking fabric. In essence, the suction in the fabric must be greater than the suction in the soil if the fabric is to be effective. To that end, the SWCC for both materials must be determined. Figure 3.1 shows the SWCC for H2Ri and the SWCC for a dense, graded base course (Lin et al., 2015). Each point on the curve requires about 1 week of testing. Consequently, it is unrealistic to determine the SWCC for every soil. Rather, values for typical soils can be used to estimate the performance of the wicking fabric.

Figure 3.1indicates two air-entry values for the wicking fabric: one is for the inter-yarn macropores, and the other is for the inner-yarn microchannels. The corresponding values are 6.7 kPa and 200 kPa, respectively. If the suction in the wicking fabric is greater than 200 kPa, air can enter into and block the microchannels in the wicking fabric, causing the wicking fabric to stop working as a drainage material for soils under unsaturated conditions. This means that if the soil suction exceeds 200 kPa, the water in the soil cannot be drained by the wicking fabric. For the soil (AB3) in Figure 3.1, that equates to 6.5% moisture content by weight. Therefore, the fabric cannot be expected to dry the soil below that value, which should not be of concern since this percentage is below the optimum water content of 8.5% and the resilient modulus of the soil is at least doubled.

Table 3.1 provides published data for sand, silt, clay, and dense graded base course. In addition, it provides the data derived from the equilibrium moisture contents from the flume. The flume data do not necessarily represent the moisture content at 200 kPa soil suction due to potential inefficiencies, but the data provide an approximation of that value, which is consistent with published data.

Lin et al. (2015) noted that the soil moisture content of dense graded materials at a soil suction of 200 kPa is approximately 2% lower than optimum for the aggregate base material used in the study, AB3. The data from the test flume discussed in Chapter 4 indicate that the effective minimum moisture content may be closer to 1% above optimum for Brown's Hill aggregate surface course (E-1), used for the study. This is likely due to the inefficiencies of moisture transfer between the soil and the fabric. In either case, the anticipated minimum moisture content is anticipated to be near optimum.

However, testing in the flume indicated that the moisture content in sand could be lowered below optimum moisture content, but not as low as the soil values reported by Fredlund and Rahardjo (1993) suggest.

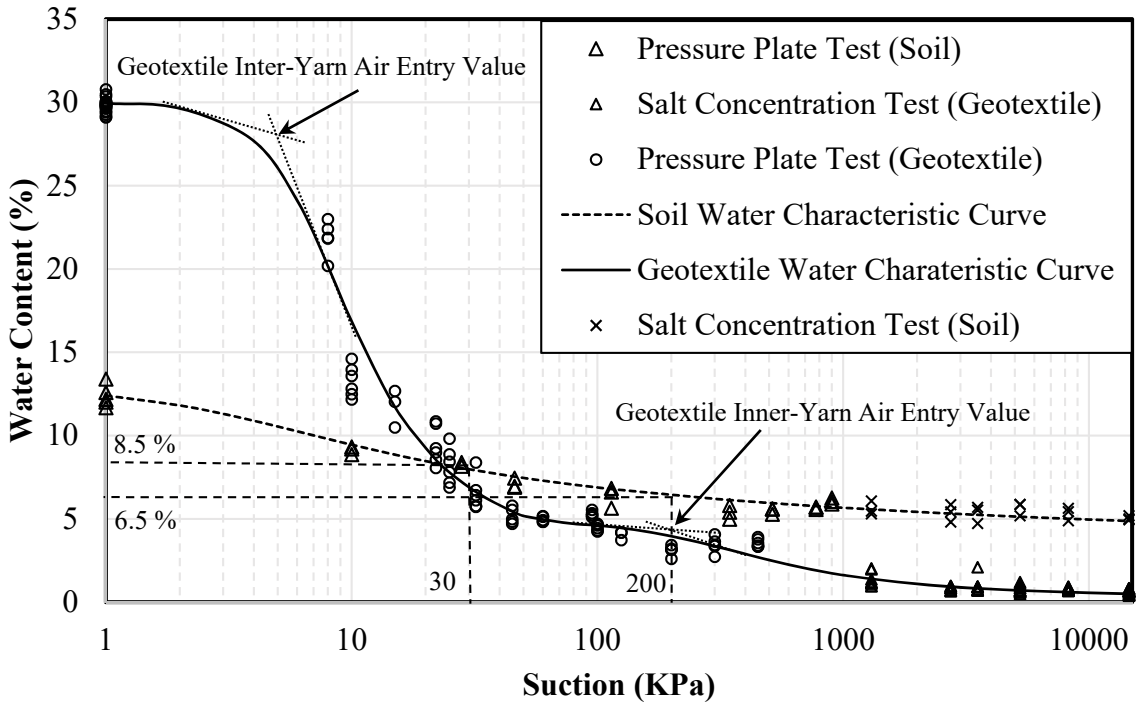

Figure 3.1 Soil water characteristic curve for H2Ri wicking fabric (Lin et al., 2015)

Table 3.1 Typical moisture content of soils with a soil suction of 200 kPa

Soil Type	**% by weight**
Clay (Fredlund)	50
Silt (Fredlund)	20
Dense Graded Base Course (Lin 2015)	6.5
Brown's Hill E-1 (estimated from flume)	9.6
FAI Crushed Sand (estimated from flume)	11.3
Sand (Fredlund)	3

CHAPTER 4 TESTING FLUME SETUP

Three test flumes were constructed to evaluate the wicking effect of the fabric. All flumes were constructed on a level grade. One flume was filled with sand, another flume was filled with Fairbanks silt (contains about 5% organic material), and a third flume was filled with Brown's Hill E-1. The schematic plot of the testing flume is shown in

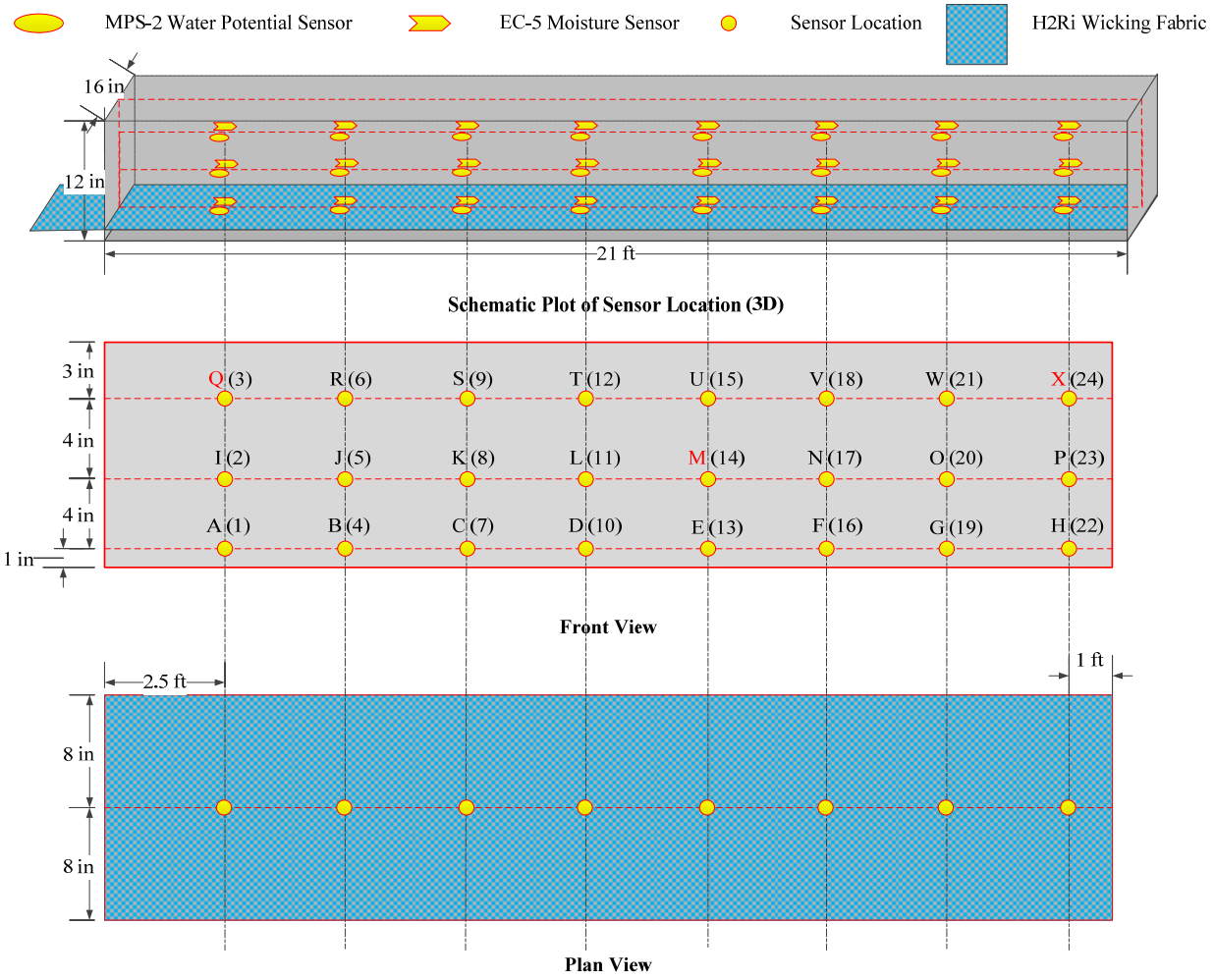

Figure 4.1. The dimensions of the first two testing flumes were 252 in. × 16 in. ×12 in. (Length × Width × Height). The third flume was 876 in. × 16 in. × 12 in. Three layers of sensors were located at depths of 1 in., 5 in., and 9 in. from the bottom to top. The wicking fabric was located at 1 in. from the bottom of the testing flume. The left side of the fabric was exposed to the open air. A 3 ft. long overlap wicking fabric started at 5 ft. from the left side of the testing flume. For the testing flume with sand, two types of sensors were used: MPS-2 water potential sensor to measure the soil suction and EC-5 moisture sensor to measure the moisture content. The moisture content sensors were marked numerically, and the water potential sensors were marked

alphabetically. Yet, since the water potential sensors did not work effectively, only the moisture sensors were used for testing flumes for silt.

The construction process started by filling the flume with 1 in. of saturated sand, as shown in Figure 4.2(a). The testing flume was first covered with a layer of plastic wrap to prevent water from flowing outside the system. Both sides of the flume walls were marked at the anticipated heights, and the sand was then flattened with a trowel to the marker. Next, the wicking fabric was put into the testing flume as shown in Figure 4.2(b). Since the fabric roll was not long enough, a 3 ft. overlap was placed at a distance of 5 ft. from the left side of the testing flume. In the case of the 73 ft flume, splices were centered at 64 in., 210 in., 354 in., 498 in., 642 in., and 786 in. The first layer of sensor was place on top of the fabric, as shown in Figure 4.2(c). One set of sensors was put at each location, and 8 sets of sensors were put in one layer. The fabric was then saturated with water before another layer of soil was put into the testing flume. Figure 4.2(d) shows the testing flume filled with 12 in. of saturated sand. The walls of the testing flume were fastened with wood plates to prevent the walls from expanding. After all the sensors were put into the testing flume, the testing system was covered with plastic wrap (see Figure 4.2[e]). Furthermore, at the left side of the testing flume, the wicking fabric was exposed to the open air so that the water inside the testing system could be wicked out.

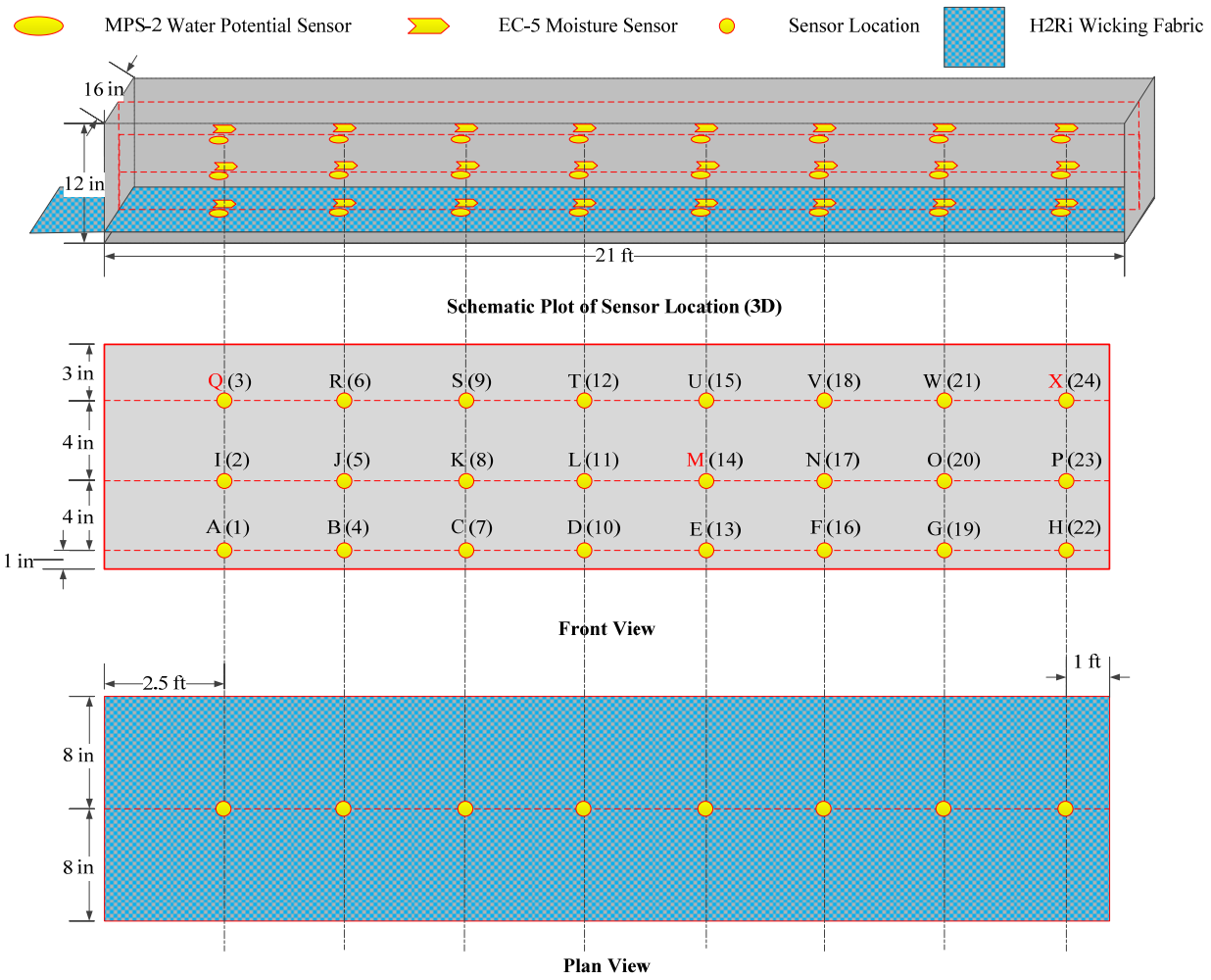

Figure 4.1 Schematic plot of testing flume and sensor location

(a) (b)

(c) (d)

(e) (f)

Figure 4.2 Testing flume construction

Figure 4.3 shows the data acquisition system. The system was composed of 1 CR1000 datalogger and 1 AM 16/32 multiplexer. The CR1000 was used to store the monitored data at a time interval of 1 hour. The AM 16/32 multiplexer provided the posts to connect, in total 48 sensors (24 water potential sensors and 24 moisture content sensors).

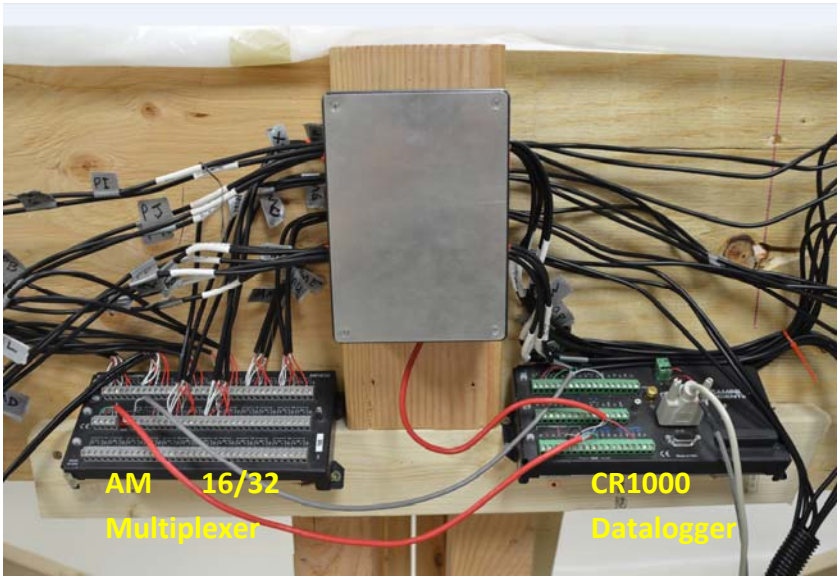

Figure 4.3 Data acquisition system

CHAPTER 5 TEST RESULTS AND DISCUSSION

Test results were categorized by three general types of tests:

1. Wicking Test: evaluating the effectiveness of the wicking fabric during the drying process.
2. Wetting Test: evaluating the effectiveness of the wicking fabric during the wetting process.
3. Rewicking Test: assessing the effectiveness of the wicking fabric during the cyclic drying-wetting process.

5.1 Case 1: Wicking Test for Sand

The wicking test for sand started at 2 P.M. on September 6, 2014. In this case, the volumetric moisture contours for the testing flume were plotted at the starting point, 2 hours, 1day, 10 days, and 1 month, as shown in Figure 5.1. At the starting point, due to gravational drainage, the moisture content decreased with increments of vertical height. The moisture content changed from 0.3 at the bottom to 0.22 at the top. Moreover, since there was a 3 ft wicking fabric overlap between 5 ft and 8 ft from the left side of the testing flume, the maximum moisture content occurred at the overlaping area. This indicated that the effectiveness of the wicking fabric dramatically diminished because of poor contact condition. After 2 hours, the moisture content at the top of the flume decreased to about 0.2. The moisture content at the left side of the flume decreased more than the right side of the flume because the wicking fabric was exposed to the open air. After 1 day, the moisture content at the top of the flume further decreased to about 0.15. Note that even though the wicking fabric effectively transported water from left to right except for the overlapping area, the effect did not disappear throughout the entire testing period. The moisture contours after 10 days and 1 month indicated that the moisture content at the top of the flume further dropped to about 0.1, and the wicking fabric worked effectively except for the overlapping area. The overlaped areas can be seen as the two wet areas in Figure 5.1(e).

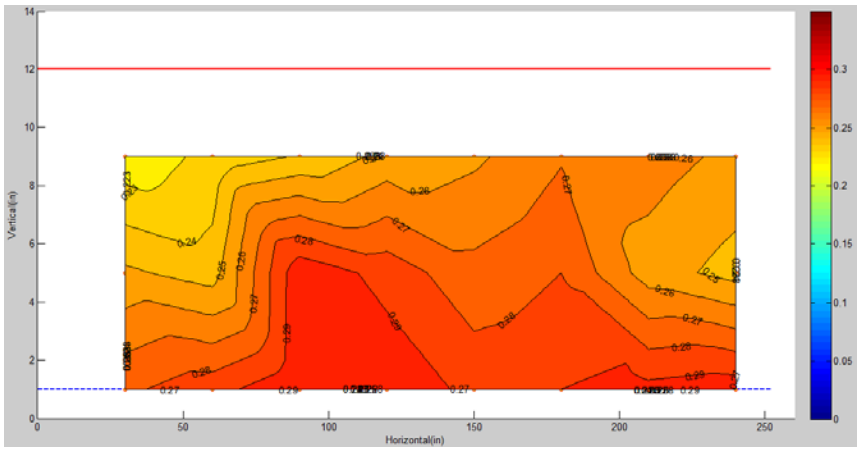

(a) Starting Point

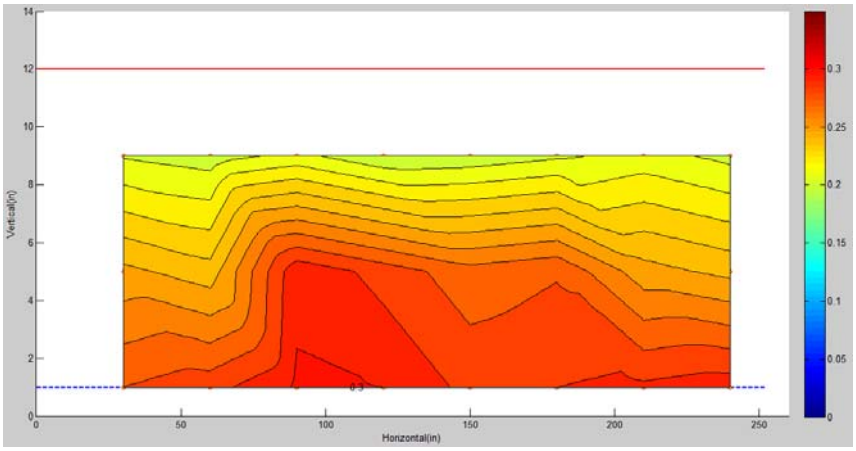

(b) 2 Hours

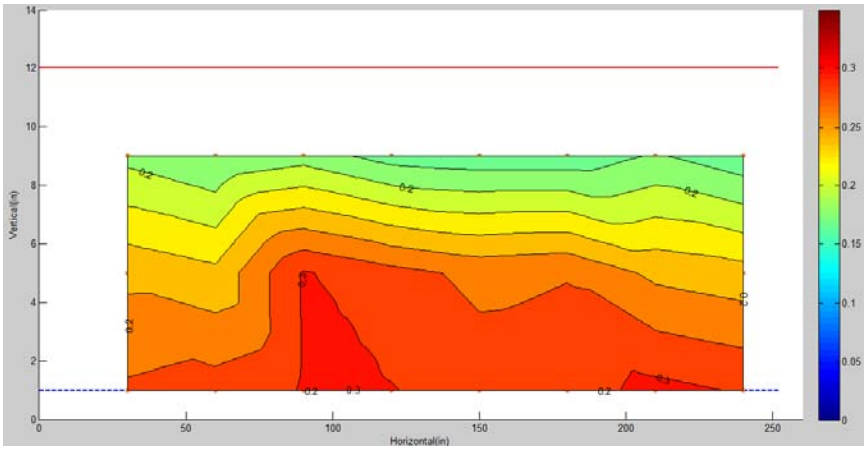

(c) 1 Day

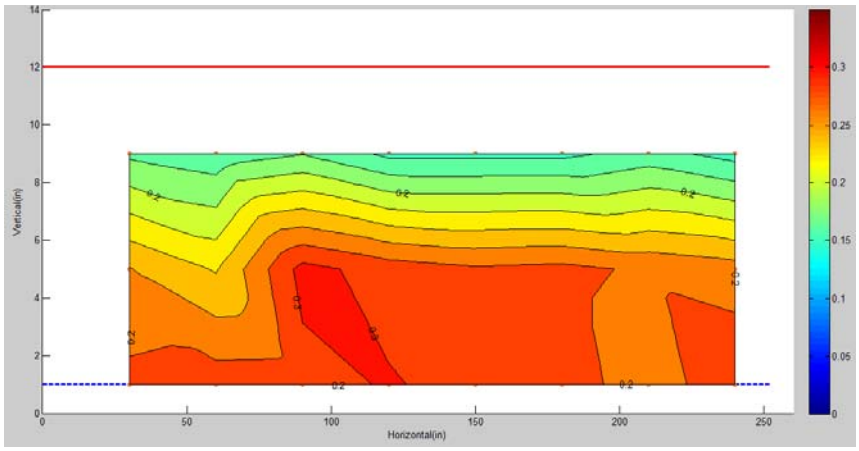

(d) 10 Days

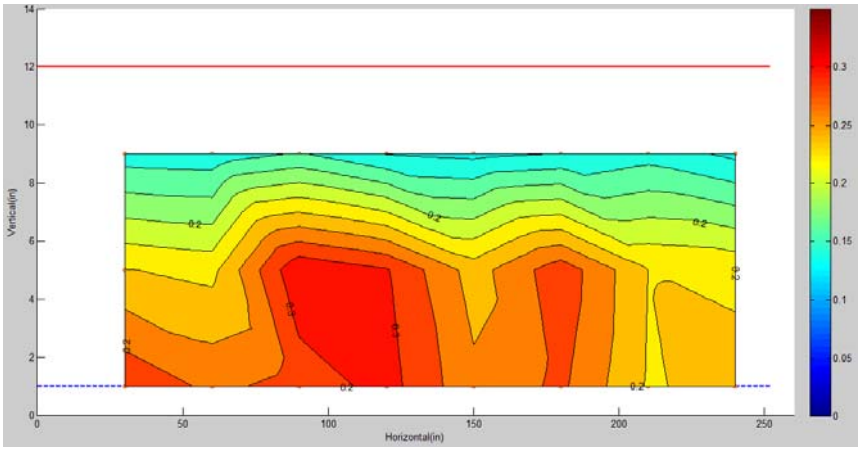

(e) 1 Month

Figure 5.1 Moisture contour for wicking test (sand)

5.2 Case 2: Wetting Test for Sand

The wetting test for sand started at 5 P.M. on November 2, 2014. The left side of the fabric was dipped into water rather than exposed to open air. Figure 5.2 shows the moisture contour for the testing flume at the starting point, 2 hours, 1 day, 10 days, and 1 month. In this case, the water flowed from left to right. At the starting point, the moisture content at the left side of the flume increased instantaneously due to the wetting of the fabric. Because of the poor connection at the overlapping area, the water could not tranport further to the right side of the flume within 1 day. After 10 days, the accumulated water at the overlapping area transported further to 180 in. The wicking fabric continued to transport water to the right side of the flume, which resulted in a slight increment in moisture content of 5% after 1 month. In general, the overlapping of the wicking fabric significantly decreased its wickability in transporting water to the right side of the testing flume.

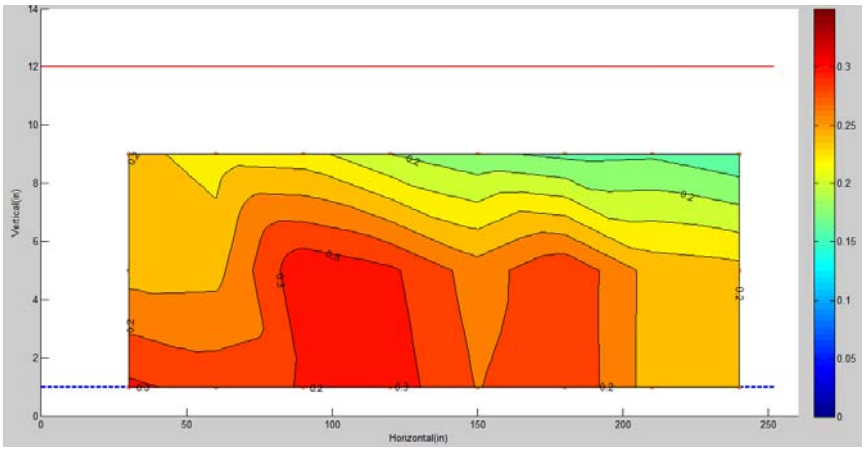

(a) Starting Point

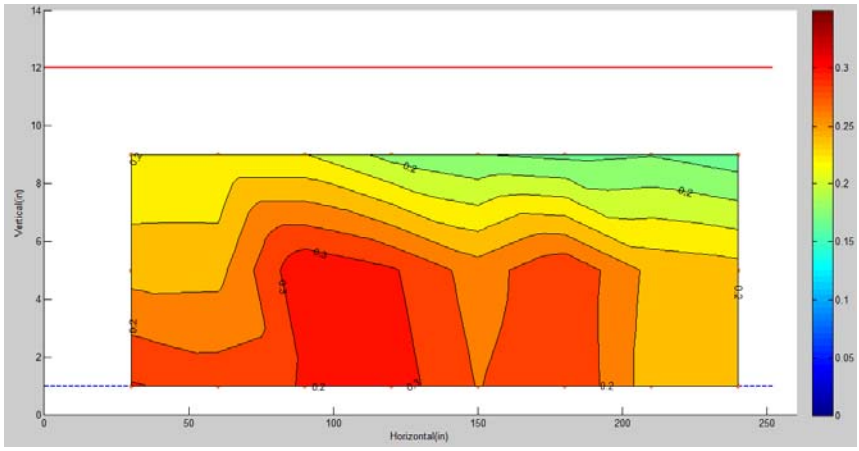

(b) 2 Hours

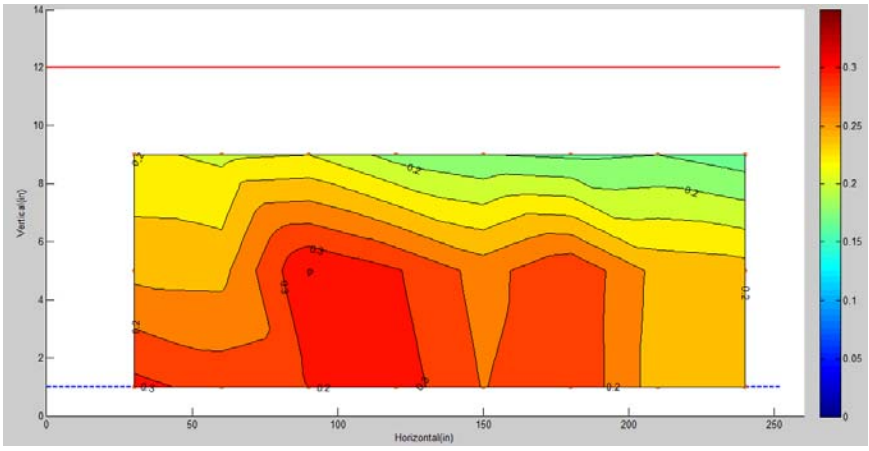

(c) 1 Day

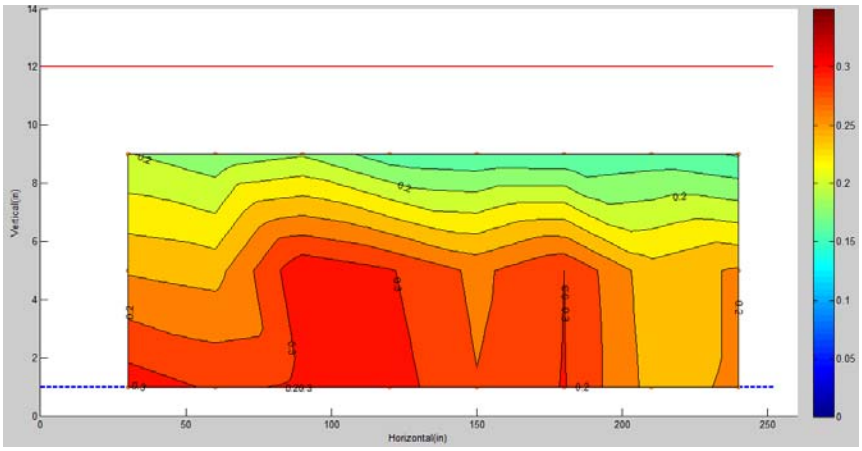

(d) 10 Days

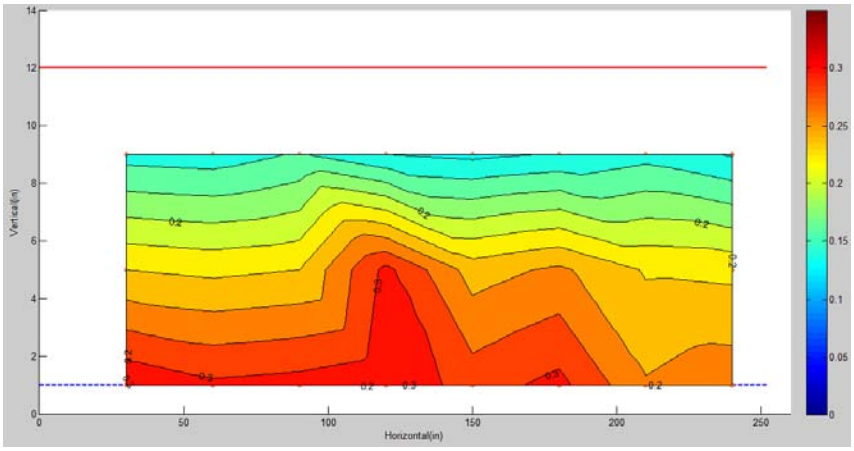

(e) 1 Month

Figure 5.2 Moisture contour for wetting test (sand)

5.3 Case 3: Rewicking Test for Sand

The rewicking test for sand started at 11 A.M. on March 13, 2015. On the right side of the testing flume, 1 ft wide of soil was removed, and a wood board was placed into the flume to prevent the soil from collapsing. In total, 10 gallons of water was poured into the gap, and the moisture content was monitored. Figure 5.3 shows the moisture contour of the testing flume at the starting point, 2 hours, 1 day, 10 days, and 1 month. Results similar to those of the wetting test were observed. The right side of the testing flume increased instantaneously after pouring in the water, and the water was transported to the overlapping area. After 10 days, the moisture content at the right side of the testing flume decreased dramatically to about 0.21 due to the combination effect of evaporation and wicking. After 1 month, the moisture content kept increasing at the overlapping area, which indicates that the effectiveness of wicking again decreased dramatically because of poor connection.

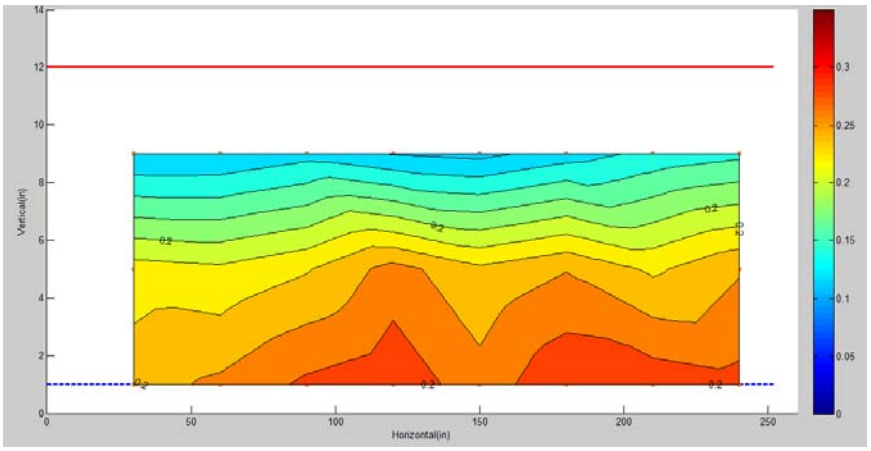

(a) Starting Point

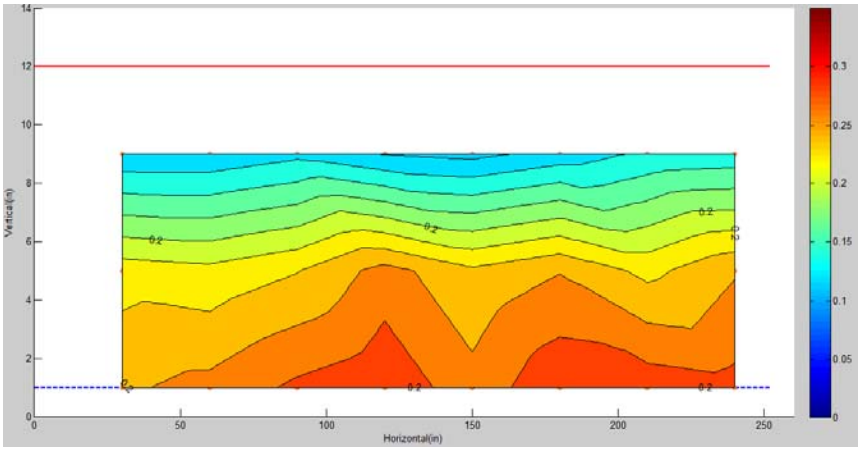

(b) 2 Hours

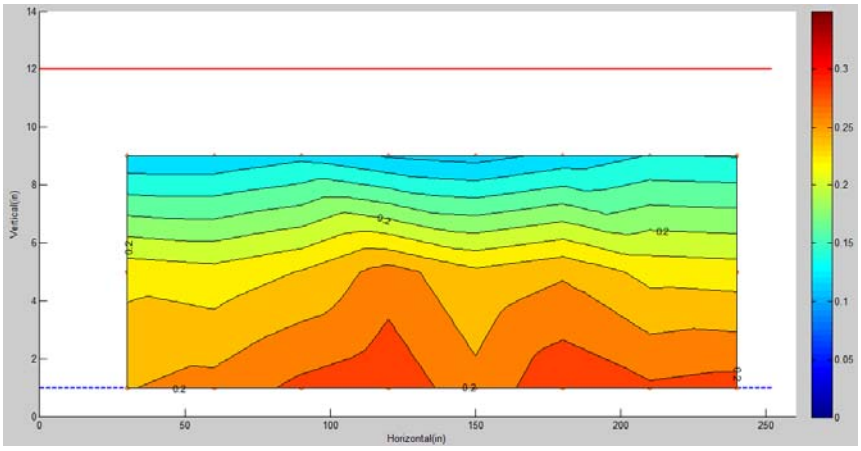

(c) 1 Day

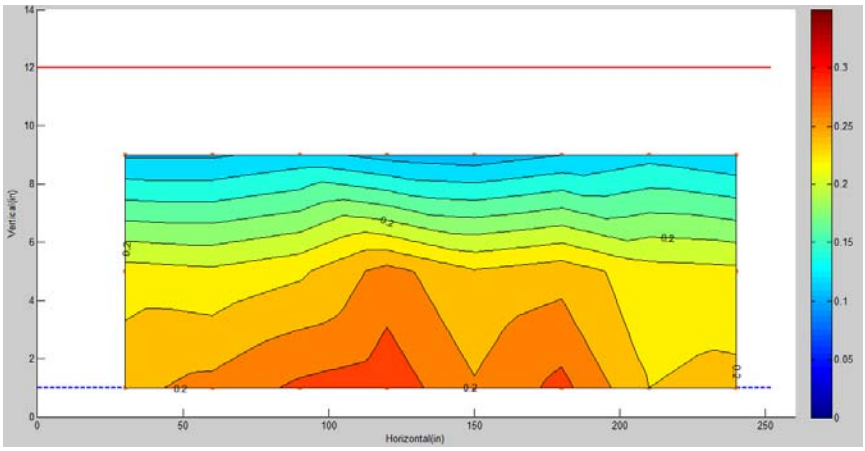

(d) 10 Days

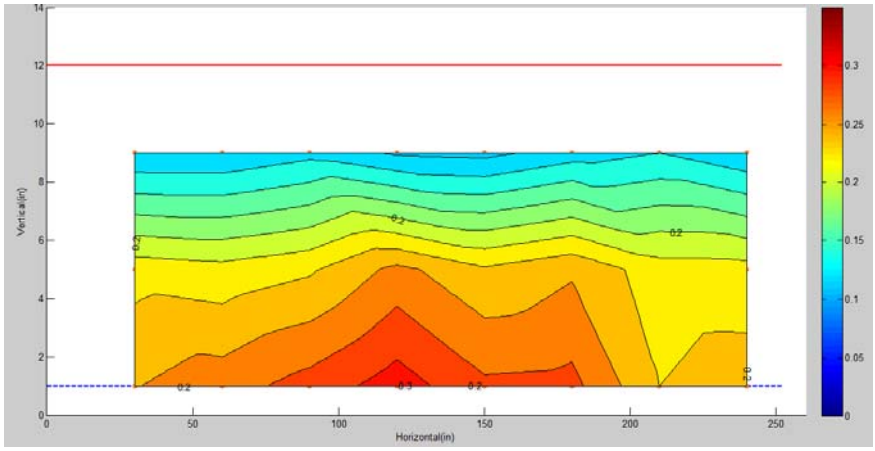

(e) 1 Month

Figure 5.3 Moisture contour for rewicking test (sand)

5.4 Case 4: Wicking Test for Silt

The wicking test for organic silt with an organic content of 5% started at 4 P.M. on December 23, 2014. The moisture content contours were plotted at the starting point, 2 hours, 1 day, 10 days, and 1 month, as shown in Figure 5.4. At the starting point, the moisture content at the left side of the flume started to decrease because of the wicking effect. Similar to the wicking test for sand, the overlapping area showed a smaller moisture content decrease due to poor connection and drainage condition. After 2 hours, the water flowed from right to left and accumulated at the overlapping area, resulting in even larger moisture content at the overlapping area. After 1 day, the blue areas indicated the mositure content was much lower than the surrounding area. Several major cracks were observed during the consolidation process, and air penetrated the soil through the cracks. Since air circulation increases the evaporation process, the moisture content decreased faster than those areas without cracks. Thus, Figure 5.4) is reasonable in explaining the drying procedure described earlier. After 10 days, the excess water at the overlapping area was gradually

wicked out, and moisture content decreased to about 2.40. After 1 month, the effect of cracks on the mositure content change was more obvious. The moisture contents at three major cracks (60 in., 147 in., and 192 in.) were much lower than the surrounding soils.

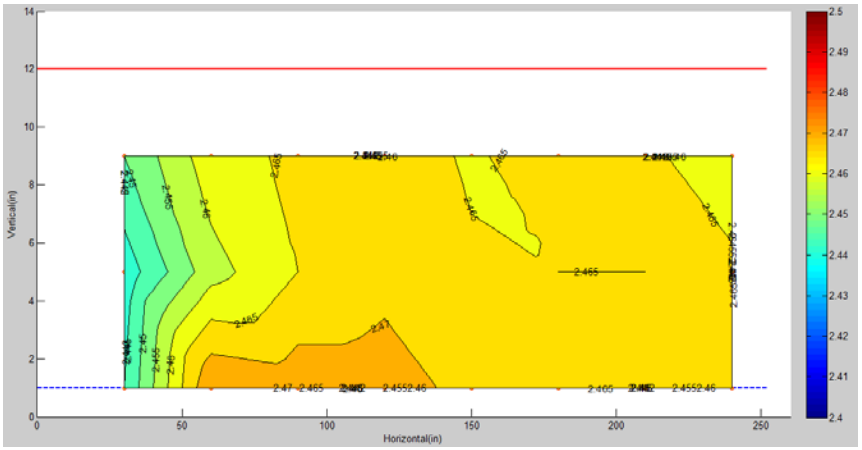

(a) Starting Point

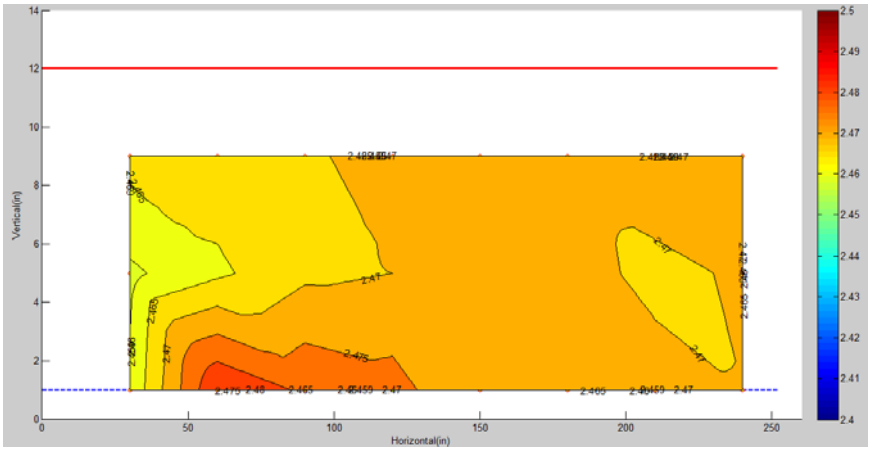

(b) 2 Hours

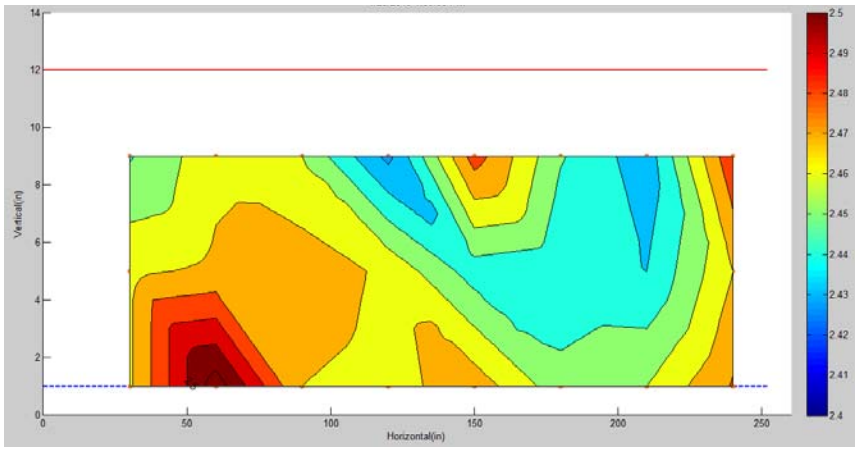

(c) 1 Day

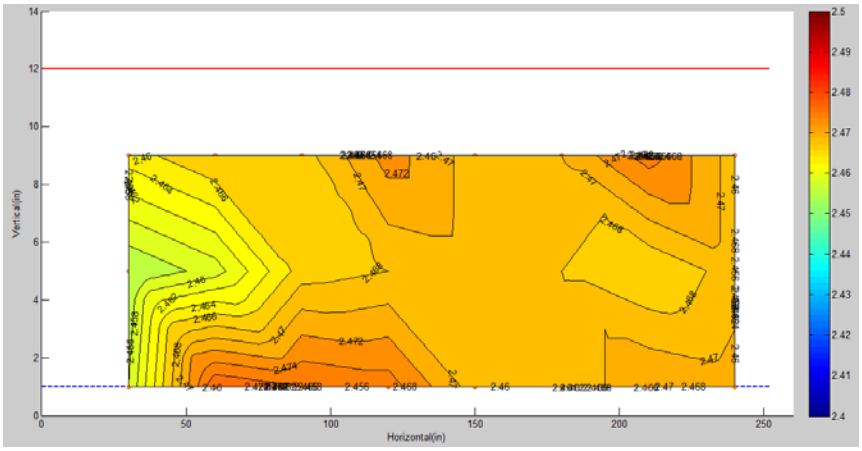

(d) 10 Days

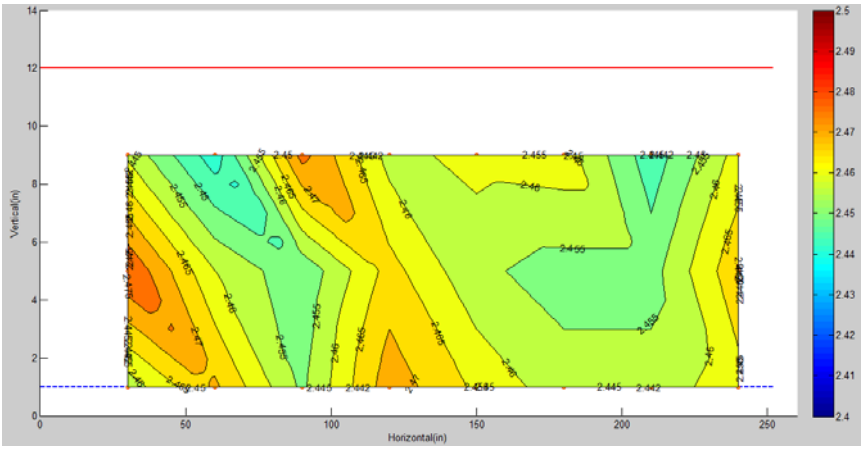

(e) 1 Month

Figure 5.4 Moisture contour for wicking test (silt)

5.5 Case 5: Rewicking Test for Silt

The rewicking test for silt started at 2 P.M. on March 12, 2014. The moisture content contours are plotted at the starting point, 2 hours, 1 day, 10 days and 1 month in Figure 5.5. Compared with the wicking test, the water flow rate for the rewicking test was much lower. After 1 day, the shape of the moisture contour did not change much. Two major reasons would cause such a phenomenon: (1) the permeability of silt iteself is much less than that of sand, and (2) the wicking paths within the fabric might have been detained by fine particles, which siginificantly reduced the water flow rate. After 1 month, the moisture contents near the three major cracks further decreased, and the amount of accumulated excess water was much less than the original test.

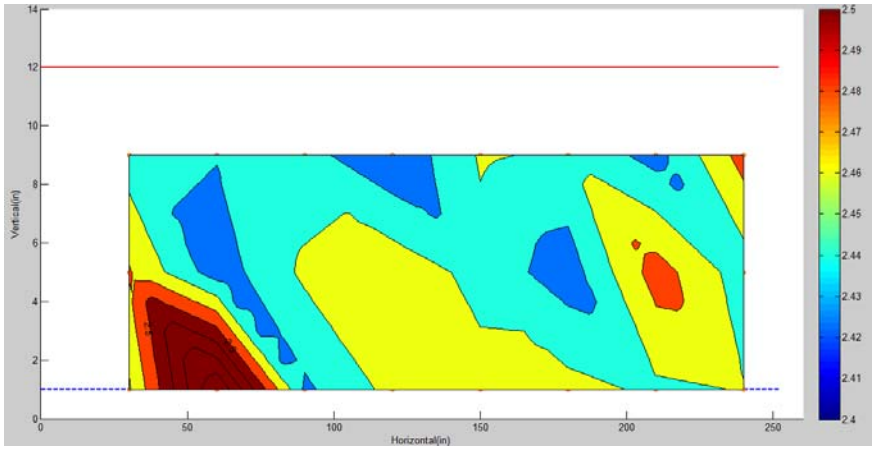

(a) Starting Point

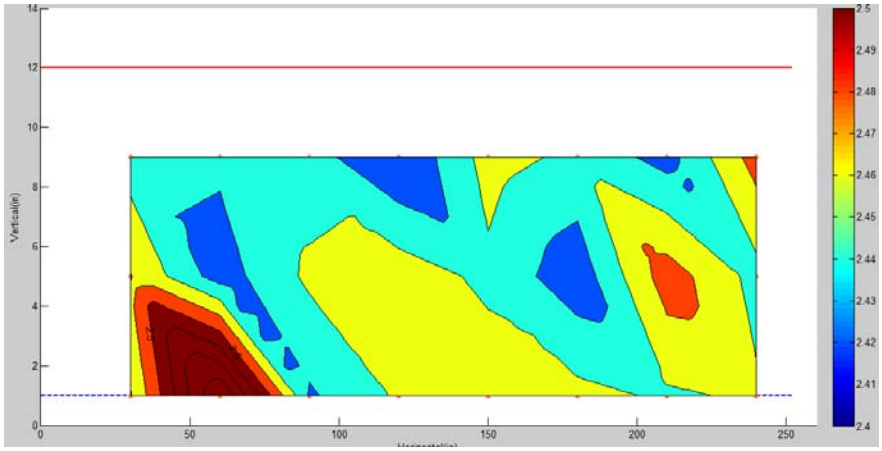

(b) 2 Hours

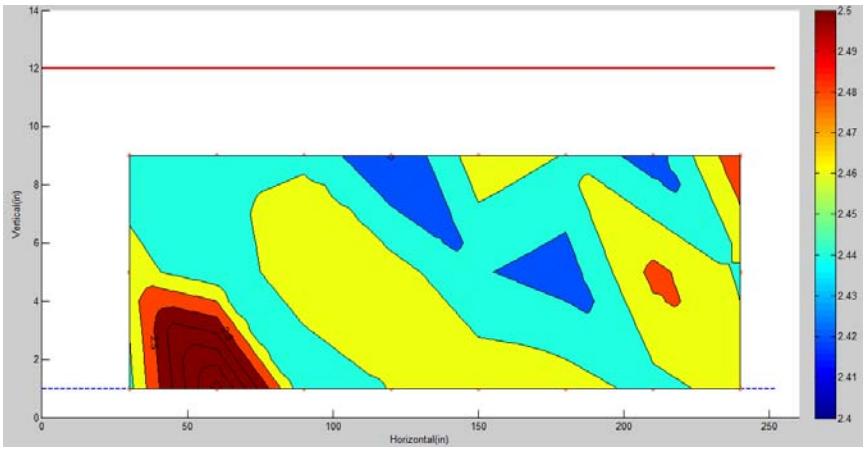

(c) 1 Day

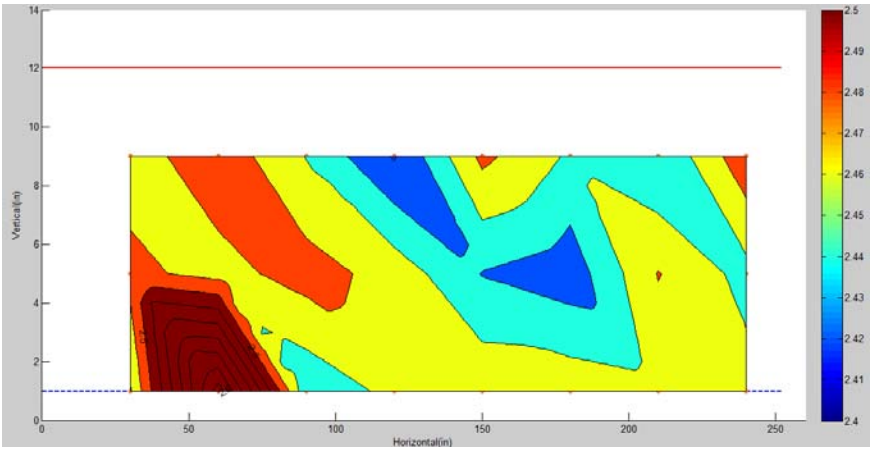

(d) 10 Days

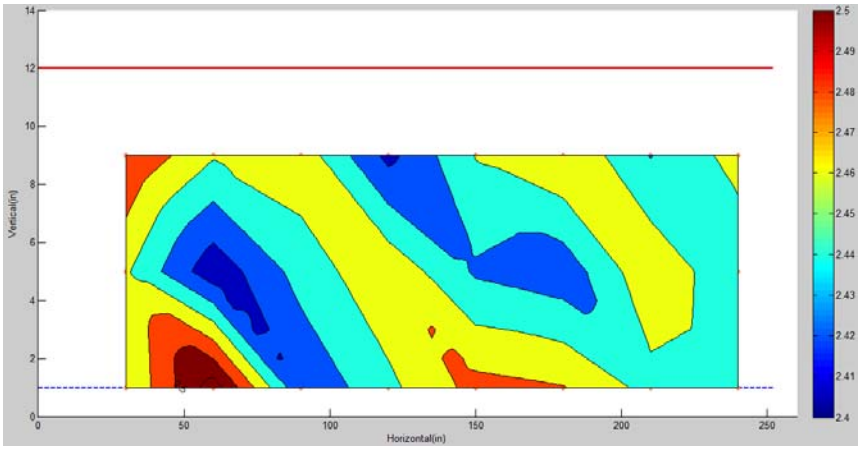

(e) 1 Month

Figure 5.5 Moisture contour for rewicking test (silt)

It is clear that organic silt has low permeability. Water added at the inlet end of the flume stabilized at about 8 inches and remained essentially at that height, clearly indicating that silt is impermeable and that the wicking fabric failed to transfer water. Photomicrographs were taken of a bundle of fibers at a magnification of 1500x. **Error! Reference source not found.** shows that the fibers were blinded by the small clay particles contained in the silt, which rendered the fabric ineffective.

Figure 5.6 Photo of organic silt and blinding of the fabric at the bottom

5.6 Case 6: 73-foot Flume with E-1

The application of H2Ri on airport runways requires the ability to transport water at least 75 feet for a 150-foot-wide embankment. To test the ability of the wicking fabric to meet that requirement a 73-foot flume was constructed (Figure 5.7). As in the previous tests, the flume was lined with 8 mil polyethylene sheeting that fully encapsulated the soil including the top.

Figure 5.7 73-foot test flume

In the previous flume, two materials were used: a well-graded sand and a highly organic silt. In order to get the performance of a material likely used in an airport surface course, a well-graded material was used with 14% fines, AASHTO Classification A-1-a (Figure 5.8).

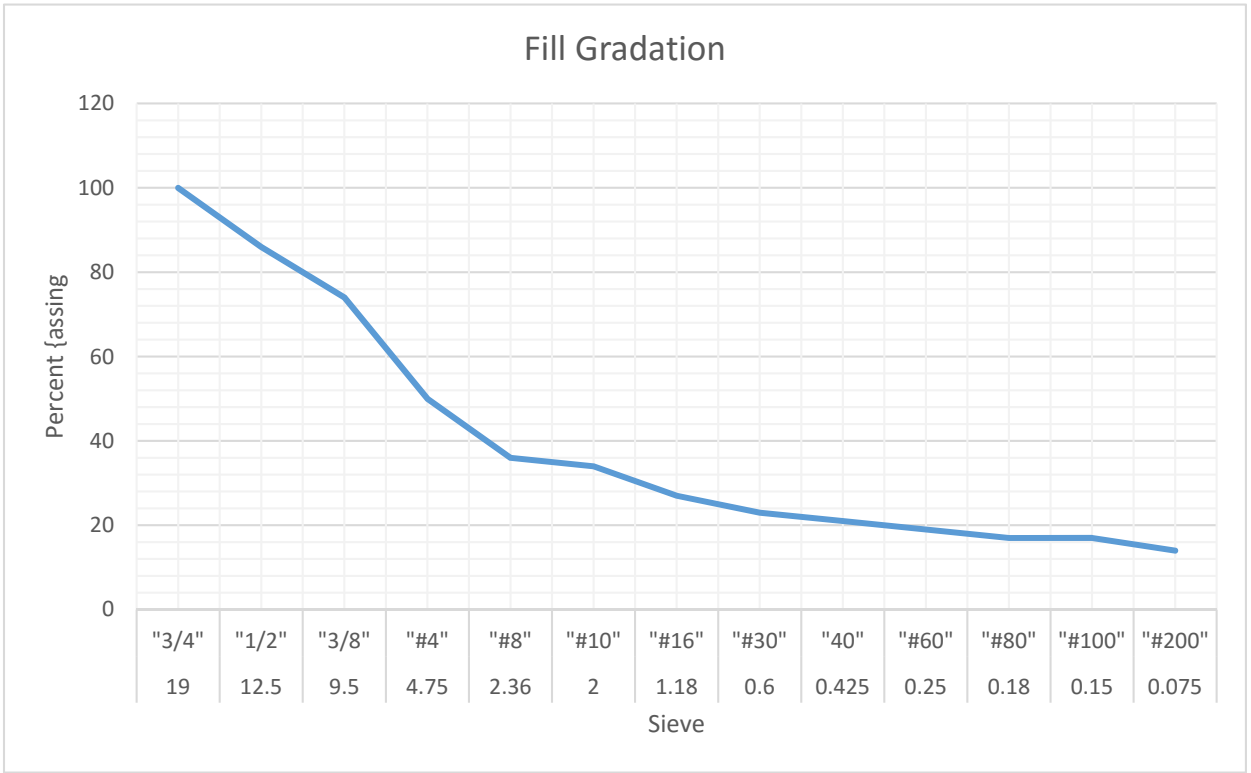

Figure 5.8 Gradation of E-1 used in 73-foot flume

As with the previous flumes, the fabric was placed 1 inch from the bottom of the soil mass. The sensors were placed in the soil column at the same vertical spacing as the previous tests, as shown in Figure 4.1. Sensor columns were placed 4 feet apart for the length of the flume, with the first sensors spaced at 4 feet from the outlet. Splices in the fabric were made using a 2-foot lap in the fabric.

E-1 was placed and compacted in the flume in 2-inch lifts. Each layer was then saturated with water and hand-compacted. Both ends of the flume were sealed to ensure that no water was lost until the start of the test. The test was started by lowering the plastic sheeting on the outlet end, exposing the fabric. During the first 48 hours, the free water drained. From that point forward, most of the water drained downward due to gravity and was then removed from the soil by the wicking fabric. The test continued for 49 days.

As can be seen from the graphics shown in Figure 5.9(a–h), the moisture content dropped consistently over time, approaching equilibrium after 4 weeks. The high moisture contents remaining in Figure 5.9(h) are over the splices. As found in previous tests, the overlapped splices are inefficient, potentially creating weak spots in the embankment. From the data collected, it is impossible to quantify the impact in performance caused by the inefficiency of the splices. As expected, the soil dried from the upper end of the flume, which indicates that the fabric was removing water.

Had the soil been allowed to dry without the H2Ri, the moisture would have been removed by surface drying and soil suction. The high fines content made the soil somewhat impermeable, thus minimizing the movement of water through gravity.

The rate of change in moisture content dropped dramatically once the volumetric water content reached 20%. Note that a minimum of 1 foot of the fabric exposed to the air remained wet throughout the test, indicating that the R2Hi wicking fabric continued to work for the duration of the test.

During teardown, it was noticed that the fabric began to dry as the upper sections of the flume were emptied, indicating that water was coming from the entire length of the flume.

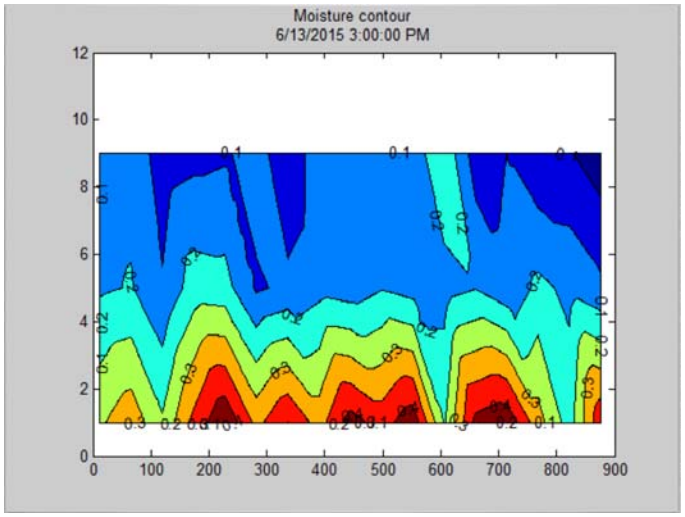

(a) Start of Test

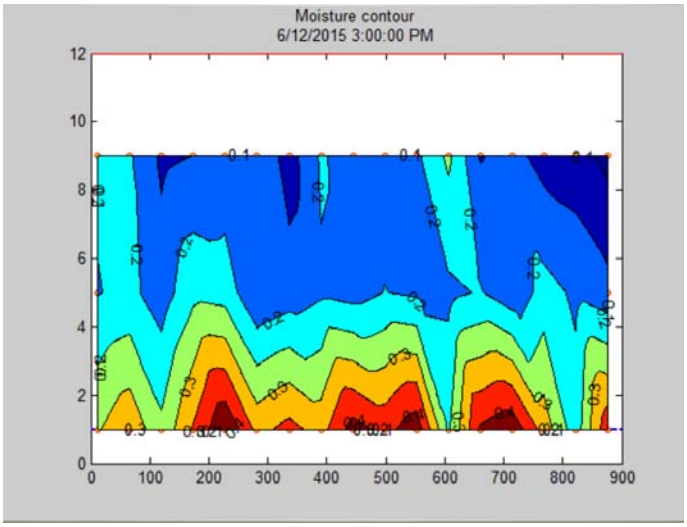

(b) After 24 hours

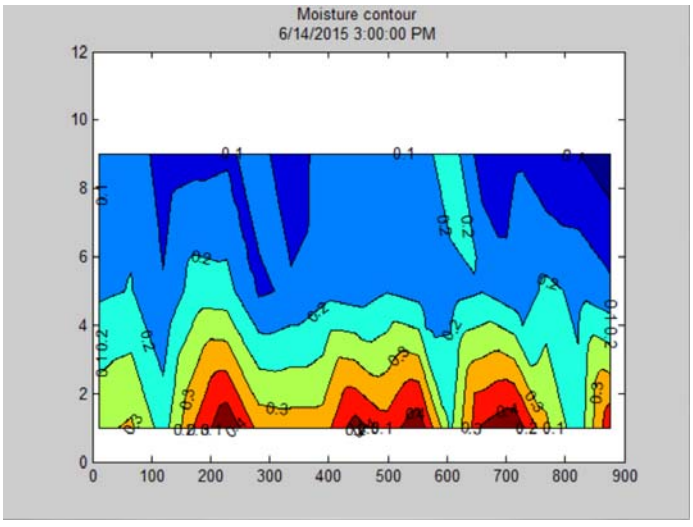

(c) After 48 hours

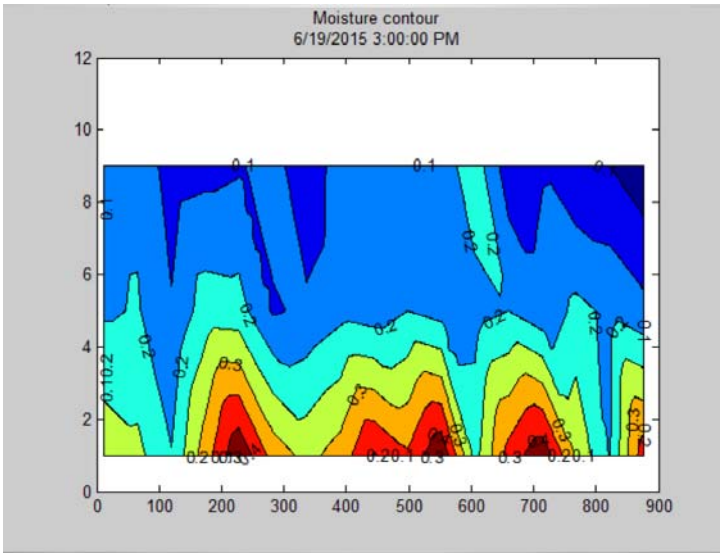

(d) After 2 weeks

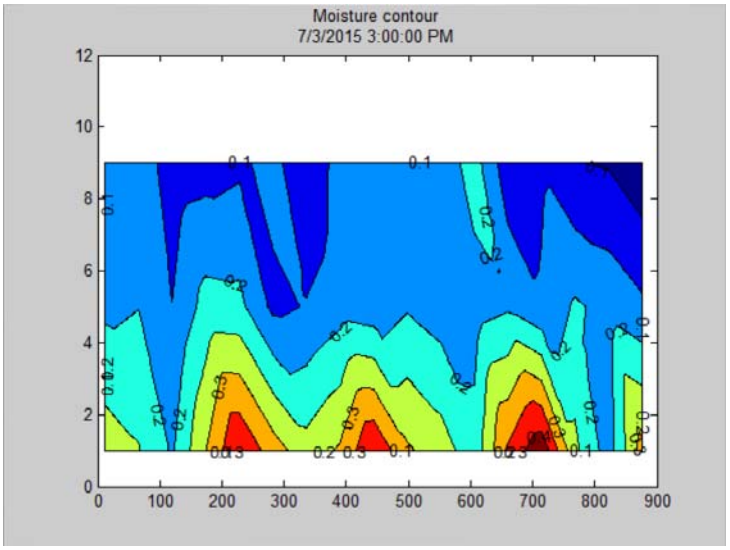

(e) After 4 weeks

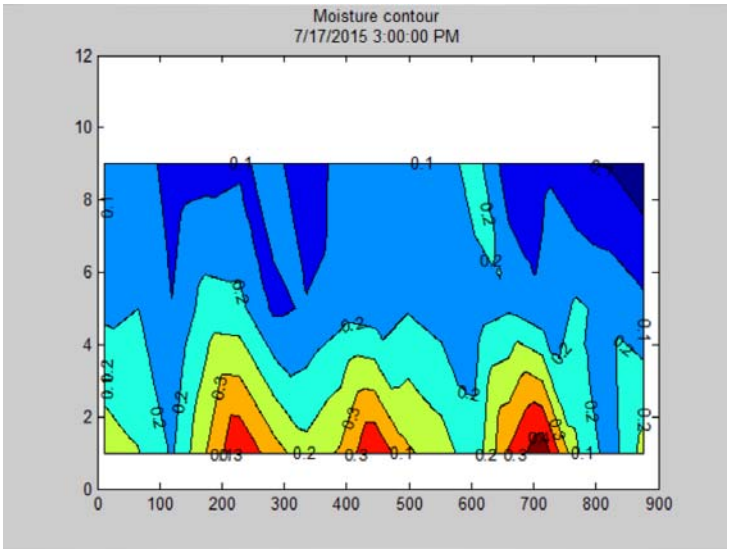

(f) After 6 weeks

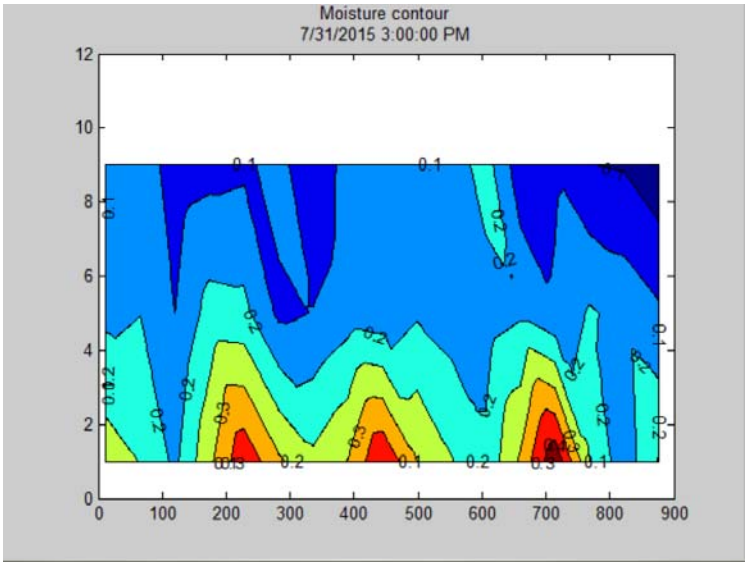

(g) After 8 weeks

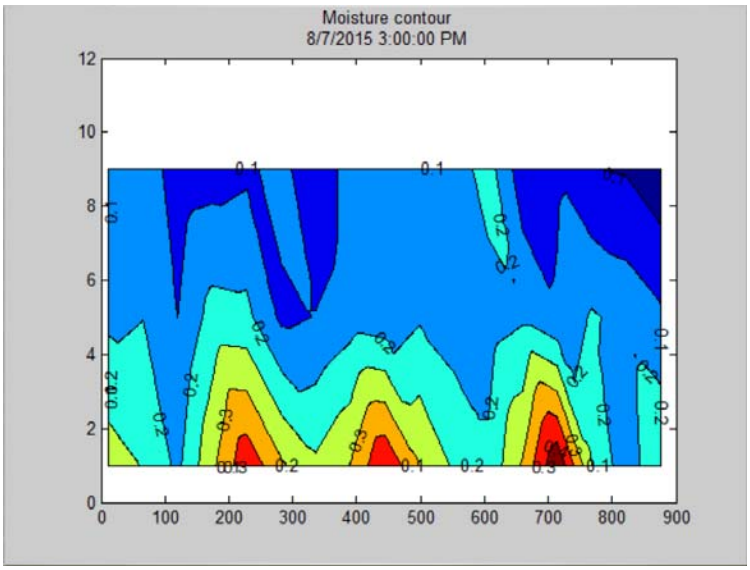

After 9 weeks; Conclusion of test

Figure 5.9 Moisture contour for rewicking test (73-foot flume with E-1)

5.7 Case 7: Introduction of Water at the Head of the Flume

On August 8, 2015 at 11:00 A.M., 1 foot of material was removed from the upper end of the flume, and 25 gallons of water was added at 12:30 P.M. This was done to simulate a point source of water at the upper end of the fabric. Figure 5.10(a) shows the effect of the addition of that water after 2½ hours. Two days later, the catch basin held about 5 gallons of water, representing the water that was removed from the soil due to gravity. The soil moisture reached equilibrium after about 3 weeks; slightly quicker that the initial test. A comparison of Figure 5.9(e) and Figure 5.10(f) shows that they appear nearly identical. Even though equilibrium appears to have been reached, the fabric remained wet until the end of the study on September 3, indicating that moisture was still being removed.

Based on the data, it appears that the wicking fabric can reduce the volumetric water content of this soil to about 20% from 40% within 3 weeks after the addition of water. At that point, it appears the soil suction is approximately equal to the suction of the fabric. However, the water content above the overlap joints is between 34% and 40%, indicating the inefficiencies of the joints.

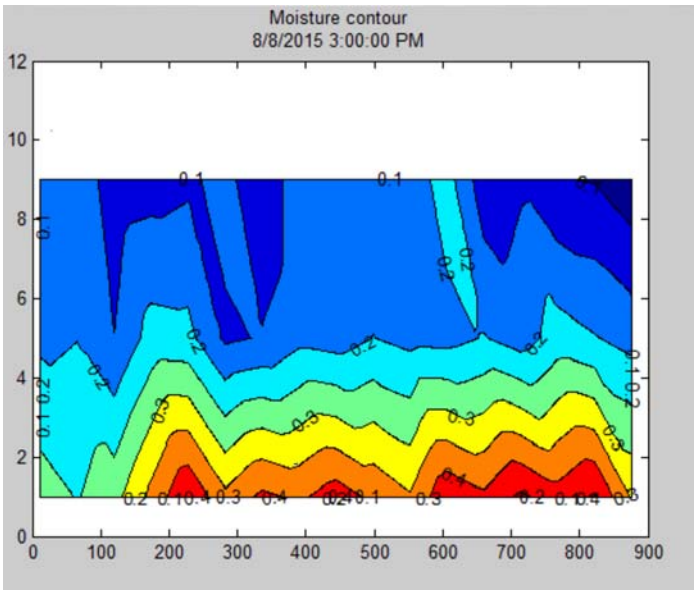

(a) 2.5 hours after addition of water

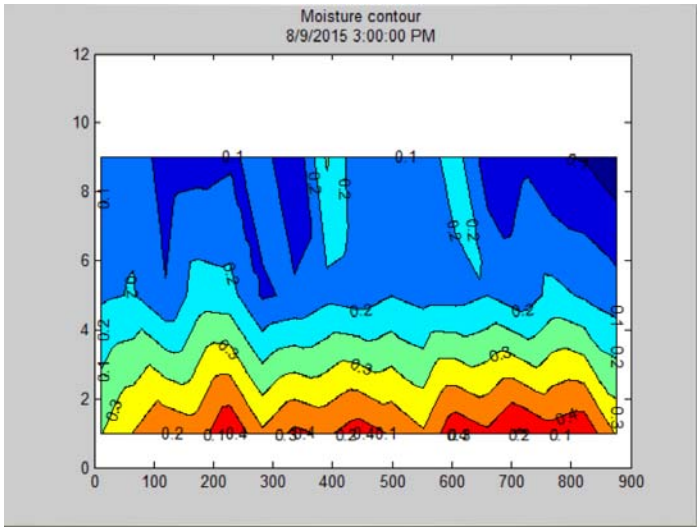

(b) After 24 hours

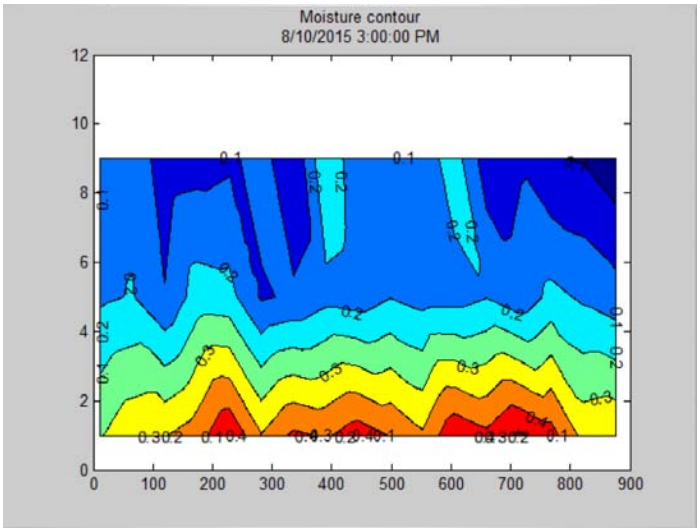

(c) After 48 hours

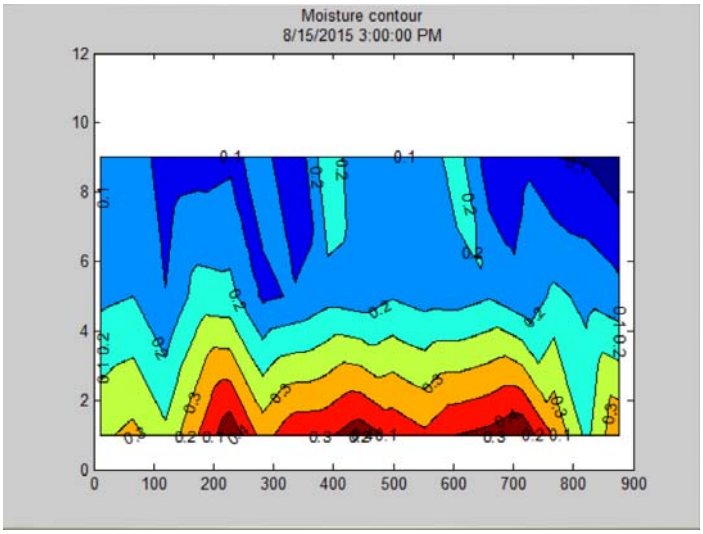

(d) After 1 week

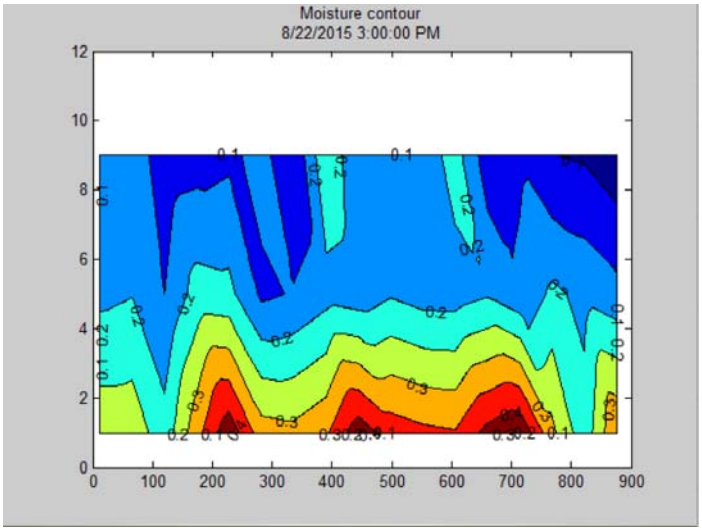

(e) After 2 weeks

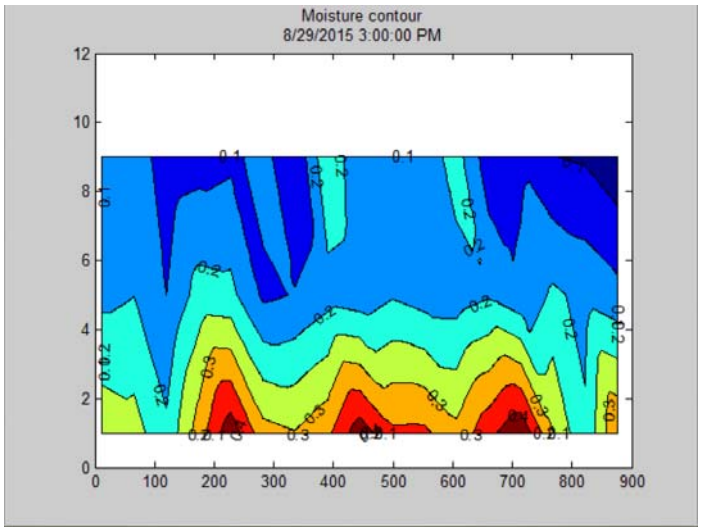

(f) After 3 weeks

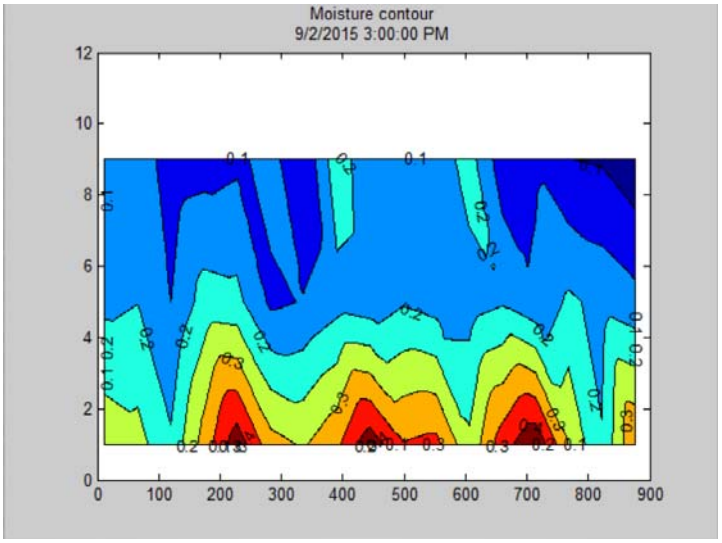

(g) After 4 weeks; conclusion of test

Figure 5.10 Moisture contour for rewicking test after the addition of water (73-foot flume with E-1)

5.8 Case 8: Estimating the Ability of Wicking Fabric to Wick Water

A generic specification for the wicking fabric is required by public agencies, because sole-sourcing material violates the state and federal procurement codes. A series of tests were performed in an effort to establish a standard.

The fabric was laid in the 120-inch flume used for previous testing between two layers of plastic film. One end of the fabric was placed in water, while the other end was exposed to air, as shown in Figure 5.11.

The test was run twice with the same sample of wicking fabric, which was dried between tests. The test results are shown in Figure 5.11. While the distance water was wicked, the time required was vastly different. In both cases, the relative humidity was between 35% and 40%, and the room temperature was between 70°F and 72°F. It was noted that the plastic underneath the fabric was wet for both tests. The authors have no definitive explanation for the differences. There is the possibility that salts in the water could have dried in the wicking channels, blocking them until they were again saturated. To test this theory, photomicrographs were taken of virgin material and material that has been wetted and dried. A photo and salt content is provided in Figure 5.12.

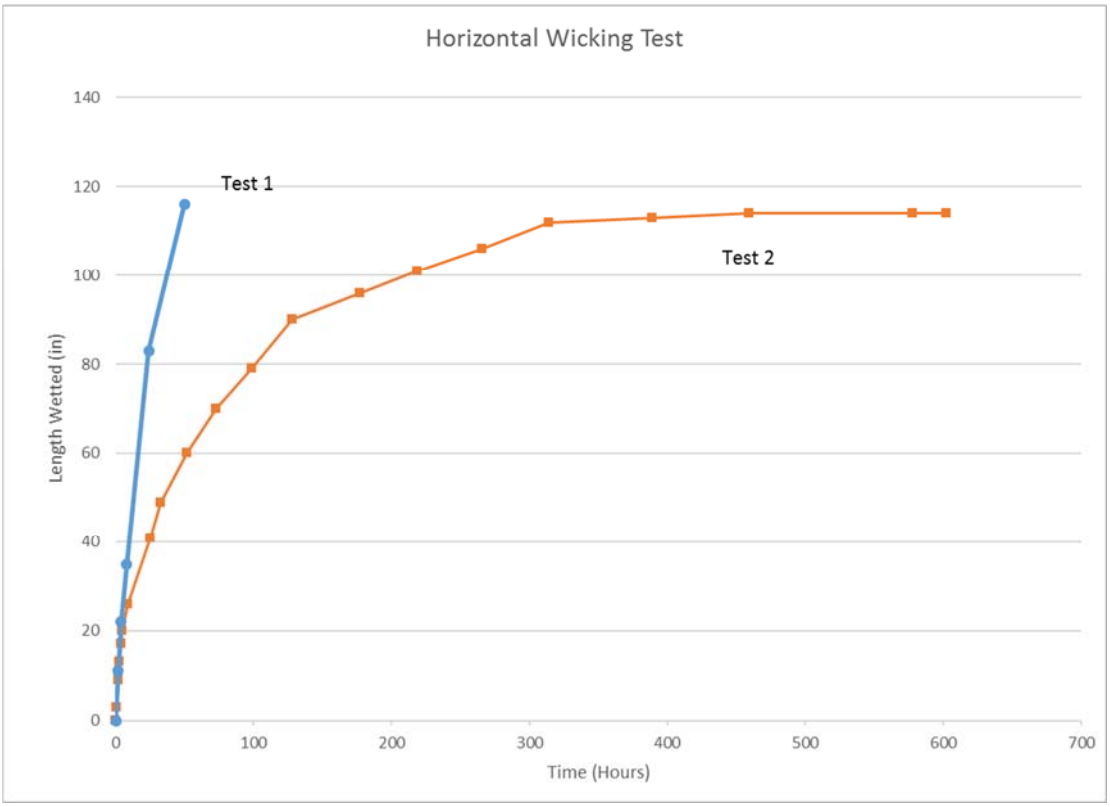

Figure 5.11 Wicking test in flume

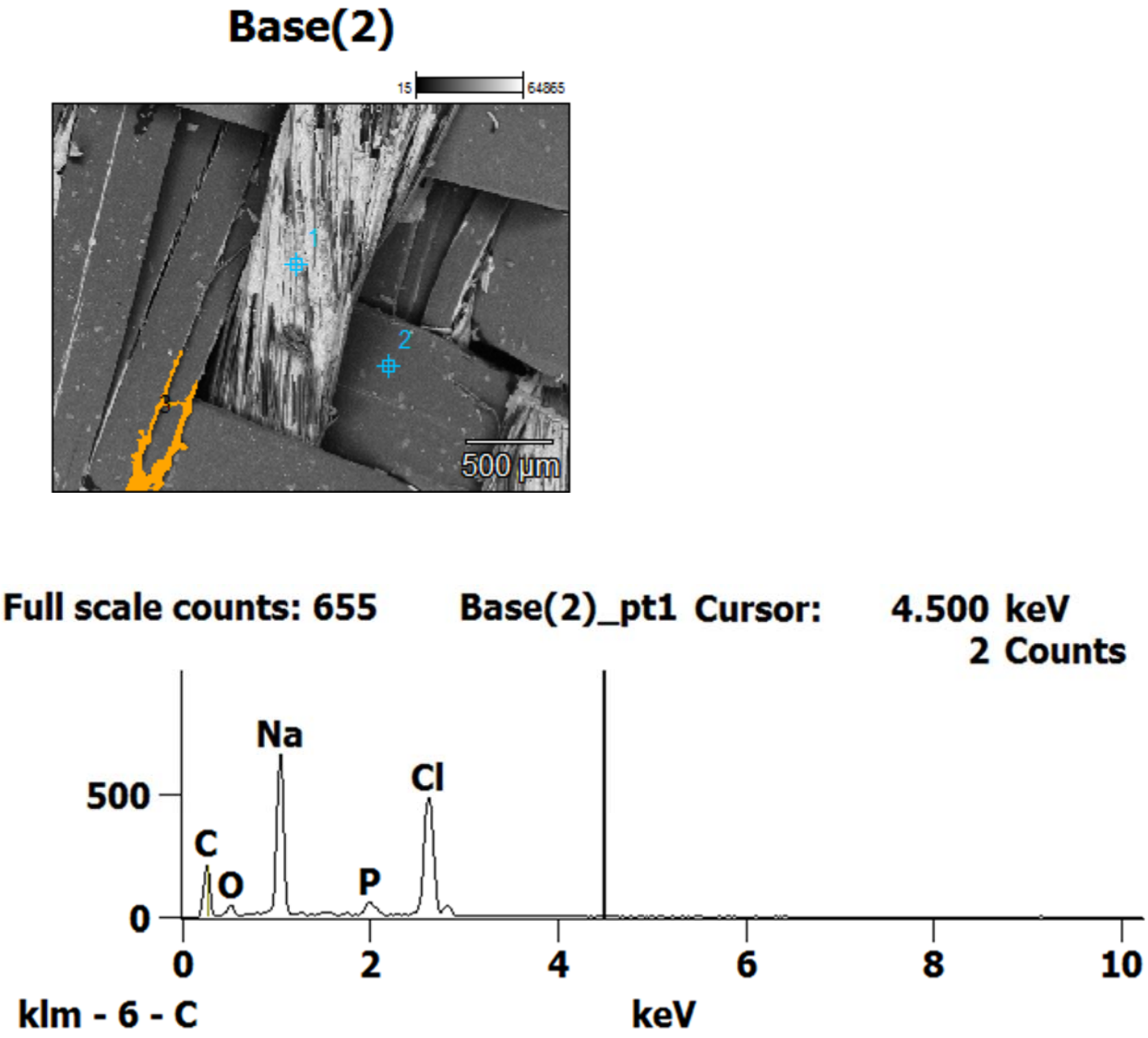

Figure 5.12 Impact of Salt on Wicking Fibers

CHAPTER 6 PROPOSED SPECIFICATIONS

One of the objectives of this study was to develop a specification for wicking fabric. Table 2.1 in the literature search shows the current TenCate specification. Zhang and Pressler (2012) performed the ASTM 1559, and exceeded the TenCate specification by twice the vertical rise specified. The test was repeated for this project. Five specimens were tested, one of which was coated in dust from the air. We chose to test the coated sample to determine if coating had an effect on the results. All samples were cut from the same roll of a 36-inch length of fabric.

The clean samples quickly wicked to maximum height of 11 inches within the specified 24 minutes of the test and did not change over 48 hours. As shown, the wicking height remained constant. The measured relative humidity in the laboratory was 16%, and the temperature was 70°F throughout the test. The dust-coated sample had a much lower wicking height of 8 inches indicating that a coating of dust reduces the efficiency of the wicking at least in the vertical tests.

It is likely that low relative humidity had an adverse effect on the wicking height. Even so, the results were reasonably consistent and near the specification. Hence, the specification appears adequate.

That said, it would be useful to require a soil characteristic curve so that the values obtained can be used for the design of the installation. While the cost for a soil characteristic curve is high, it need only be run once, unless the design of the fabric changes.

CHAPTER 7 SUMMARY AND CONCLUSIONS

Based on the literature we anticipated that H2Ri performs well in gravels, sands and silts. However, when tested in organic silt with an organic content of 5% the wicking fabric was immediately blinded and ceased to perform. This result was confirmed by two methods first by supplying clear water at the upstream end of the fabric. The fabric failed to remove any of the water. The fabric at the outlet of the flume remained completely dry throughout the test. The photomicrographs of the wicking bundles showed the fibers were coated with the organic clay contained in the silt (Figure 7.1).

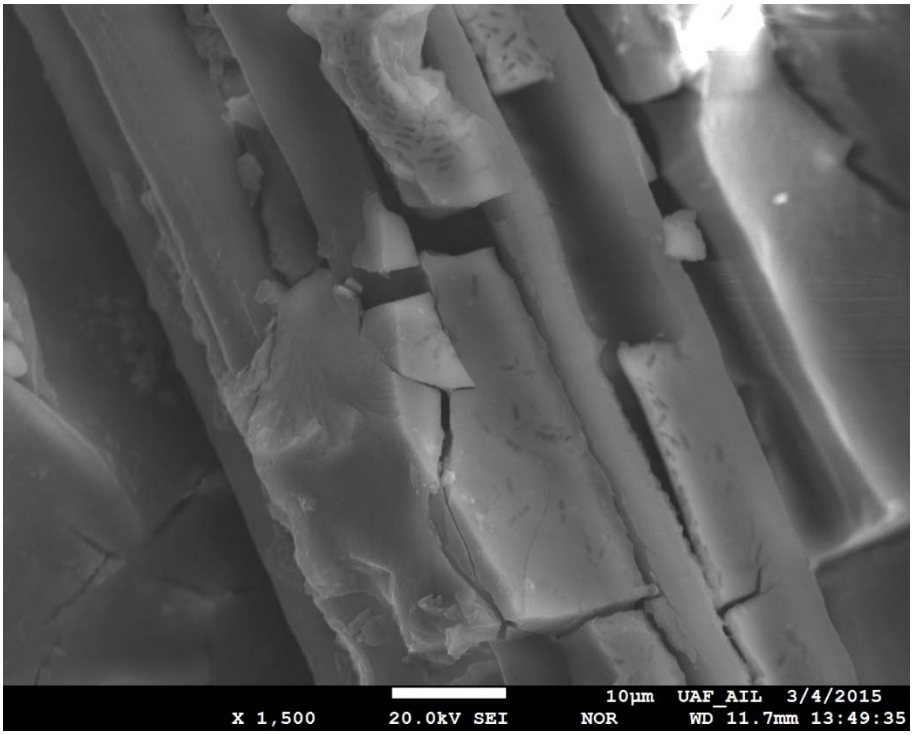

Figure 7.1 1500x photomicrograph of wicking fiber bundle blinded by organic silt

As expected, H2Ri performed well in the flume containing the sand during all three test phases. In each case, the data indicated the fabric was capable of removing any water that was able to migrate to it.

Perhaps the most telling indicator of the effectiveness of the wicking fabric was shown in the wetting test for the sand (Case 2), where H2Ri moved free water into the sand up to the splice.

The data from all of the tests in the sand flume indicated that the splices in the fabric were inefficient. This finding was confirmed during disassembly of the flume. The soil beneath the splice was fully saturated, and free water was visible on top of the fabric.

Based on the tests, H2Ri can be expected to work well in free-draining soil such as sands and sandy gravels and silts. However, H2Ri should not be used in organic silts. These soils represent extremes. Unfortunately, no firm conclusions about clays or soils containing clay can be drawn with this data, since organic clays have properties that are not necessarily indicative of other clays. It is likely, however, that H2Ri will not be effective in impermeable soils, since water cannot readily get to the fabric.

The test as to whether a soil will benefit from H2Ri can be based on the soil suction. Once the soil suction exceeds 200kPa the H2Ri will no longer be effective. Therefore, if there is a question as to whether the H2Ri will work with a soil, it is suggested that a soil-water characteristic curve be developed for the soil to determine at what moisture content the soil suction exceeds 200kPa.

Splices are a concern due to the inefficiencies observed. There are two basic alternatives for resolving this issue. The first is to consider weaving the wicking fibers in the longitudinal direction of the fabric rather than the transverse direction. This would eliminate the need for a splice. The second is to develop an effective splice. The 3-foot simple overlap used in this experiment was not effective. It is doubtful that a sewn joint would be better.

Tests in the 73-foot flume showed that H2Ri can wick over long distances, which makes it attractive for use in muli-lane applications and for airports. However, as was shown in previous tests, the splices are inefficient and warrant improvement.

The development of the soil water characteristic curve provides the basis for estimating the effectiveness of wicking fabric. The maximum usable soil suction generated by the fabric is 200 kPa. If the soil suction equals or exceeds that value, H2Ri will no longer be effective. Using a curve developed for dense graded base courses, the fabric can reduce the soil moisture to about 2% below the optimum soil moisture content under ideal conditions. However, data from the flumes indicate that the practical soil moisture content for dense graded materials is about 1% above optimum. This indicates that the moisture transfer from the soil to the fabric is somewhat less than 100% efficient, which does not reduce the value of the fabric significantly, but is an important inefficiency to recognize.

Since ASTM C1559 is similar to the wicking tests devised by the project team and since it gives similar results, accepting the test as a standard for wicking fabrics is reasonable. Even though the tests performed by the project team were run well below the required 50% relative humidity, the test results are near the values specified by TenCate.

REFERENCES

AASHTO. 1993. "AASHTO Guide for Design of Pavement Structures." *American Association of State Highway and Transportation Officials (AASHTO),* Washington DC, USA.

Anderson, D. A., R. S. Huebner, J. R. Reed, J. C. Warner, and J. J. Henry. 1998. "Improved Surface Drainage of Pavements." *National Cooperative Highway Research Program (NCHRP)*, Project No. 1-29.

Aravin, V. I., and S. N. Numerov. 1953. *Theory of Fluid Flow in Undeformable Porous Media.* Gostekhizdat, Moscow, USSR.

ASTM. 2015. "Standard Test Method for Determining Wicking of Fibrous Glass Blanket Insulation". C 1559-15. Conshohocken, PA.

Barber, E. S., and C. L. Sawyer. 1952. "Highway Subdrainage." *Public Roads*, 26(12).

Brown, S. A., S. M. Stein, and J. C. Warner. 2001. "Urban Drainage Design Manual, Hydraulic Engineering Circular 22," 2nd ed., *Federal Highway Administration,* Publication No. FHWA-NHI-01-021.

Casagrande, A. 1931. "Discussion of Frost Heaving," *Proceedings, Highway Research Board*, 11: 163–172.

Casagrande, A. 1947. "Classification and Identification of Soils." *Proceedings, American Society of Civil Engineers*, 73(6): 283.

Cedergren, H. R. 1974. *Drainage of Highway and Airfield Pavements*. John Wiley & Sons, New York.

Cedergren, H. R., J. A. Arman, and K. H. O'Brien. 1973. "Development of Guidelines for the Design of Subsurface Drainage Systems for Highway Pavement Structural Sections, Final Report." *Federal Highway Administration*, Washington, DC, February.

Chamberlain, E. J. 1987. "A Freeze-Thaw Test to Determine the Frost Susceptibility of Soils." *U.S. Army Corps of Engineers, Cold Regions Research and Engineering Laboratory (CRREL),* Special Report: 87-1.

Csathy, T. I., and D. L. Townsend. 1962. "Pore Size and Field Frost Performance of Soils." *Highway Research Board Bulletin*, 331: 67–80.

FHWA (1980). "Highway Subdrainage Design." *Federal Highway Administration*, Publication No. FHWA-TS-80-224, U.S. Department of Transportation.

National Cooperative Highway Research Program (NCHRP). (2004). "Guide for Mechanistic Empirical Design of New and Rehabilitated Structures." NCHRP Report 01-37A. *Transportation Research Board*, Washington, DC.

Fredlund, D. G., and H. Rahardjo. 1993. *Soil Mechanics for Unsaturated Soils*. John Wiley & Sons.

Han, J., and X. Zhang. 2014. "Recent Advances in the Use of Geosynthetics to Enhance Sustainability of Roadways." *20th International Conference on Advances in Civil Engineering for Sustainable Development*, Suranaree University of Technology, Nakhon Ratchasima, Thailand, pp. 29–39.

Polubarinova-Kochina and Ya, P. (1952). “Theory of Ground Water Movement (in Russian).” Gostekhizdat, Moscow; English Translation by R. J. M. De Wiest, *Princeton University Press*, Princeton, NJ, 1962.

Lane, K. S., and D. E. Washburn. 1946. “Capillary Tests by Capillarimeter and by Soil Filled Tubes.” *Proceedings, Highway Research Board*.

Lin, C. and Zhang, X. (2015). “Comprehensive Material Characterization for a Granular Base Installed with Geotextile Incorporating Wicking Fabrics”. (Under Review)

Mallela, J. L., TiTus-Glover, and M. I. Darter. 2000. “Considerations for Providing Subsurface Drainage in Jointed Concrete Pavements.” *In:* Transportation Research Record 1709, *TRB National Research Council*, Washington, DC, pp. 1–10.

MEPDG. 2004. “National Cooperative Highway Research Program, Transportation Research Board and National Research Council. Mechanistic-Empirical Design of New and Rehabilitated Pavement Structures.” *National Cooperative Highway Research Program*, NCHRP Project 1-37A Report, National Research Council. Washington, DC.

Muskat, M. 1946. *The Flow of Homogeneous Fluids through Porous Media.* J. W. Edwards, Publisher, Ann Arbor, Michigan.

Palmeria, E. M., and M. G. Gardoni. 2000. “Influence of Partial Clogging and Pressure on the Behavior of Geotextiles in Drainage System.” *Geosynthetics International*, 7: 403–431.

Polubarinova-Kochina, and P. Ya. 1952. *Theory of the Motion of Ground Water*. Gostekhizdat, Moscow, USSR.

Rechart, F. E. 1957. “Review of the Theories for Sand Drains.” Transactions, *American Society of Civil Engineers*, 124.

Rutledge, P. C., and S. J. Johnson. 1958. “Review of Uses of Vertical Sand Drains.” Bulletin 173, *Highway Research Board*, Washington, DC.

“Standard Test Method for Determining Wicking of Fibrous Glass Blanket Insulation”. C 1559-15. Conshohocken, PA.

Taber, S. 1930a. “The Mechanics of Frost Heaving.” *Journal of Geology*, 38: 303–317.

Taber, S. 1930b. “Freezing and Thawing of Soils as Factors in the Destruction of Road Pavements.” *Public Roads*, 11(6): 113–132.

Takagi, S. 1978. “Segregation Freezing as the Cause of Suction Force in Ice Lens Formation.” *Cold Regions Research and Engineering Laboratory (CRREL),* Report No. 78-6, pp, 12.

Takagi, S. 1980. “The Adsorption Force Theory of Frost Heaving.” *Cold Regions Science and Technology*, 3: 57–81.

Taylor, M. A., and N. P. Khosla. 1983. “Stripping of Asphalt Pavement-State of the Art.” *In:* Transportation Research Record 911, *TRB National Research Council*, Washington, DC, pp. 150–158.

Wang, F., J. Han, X. Zhang, and J. Guo. 2015. “Laboratory Test to Evaluate Effectiveness of Wicking Fabric in Soil Moisture Reduction.” *Journal of Geotechnical and Geoenvironmental Engineering*, ASCE. (Under Review)

Zhang, X., & Belmont, N. (2011). "Use of Wicking Fabric to Help Prevent Differential Settlements in Expansive Soil Embankments." *Geo-Frontiers*, 3915-3924.

Zhang, X., and W. Presler. 2012. "Use of H2Ri Wicking Fabric to Prevent Frost Boils in the Dalton Highway Beaver Slide Area, Alaska." *Alaska University Transportation Center (AUTC) Project Report*, No. RR10.02 and 510020, August 2012.

Zhang, X., W. Presler, L. Li, D. Jones, and B. Odgers. 2014. "Use of Wicking Fabric to Help Prevent Frost Boils in Alaskan Pavements." *Journal of Materials in Civil Engineering*, ASCE, pp. 739.

Zornberg, J. G., B. Odgers, G. H. Roodi, and M. M. Azevedo. 2013. "Advantages and Applications of Enhanced Lateral Drainage in Pavement Systems." *Proceedings of the 2nd African Regional Conference on Geosynthetics*, GeoAfrica 2013, 18–20 November, Accra, Ghana, pp. 539–548.